nature portfolio

Peer Review File

Chiral laser gyroscopes breaking the lock-in limit

Corresponding Author: Dr Franco Nori

This file contains all reviewer reports in order by version, followed by all author rebuttals in order by version.

Version 0:

Reviewer comments:

Referee #1

(Remarks to the Author)
The manuscript 'Chiral Laser Gyroscopes Breaking the Lock-in Limit' presents an interesting approach to overcoming one of the longstanding challenges in ring laser gyroscopes (RLGs): the lock-in phenomenon. In conventional RLGs, backscattering from mirror imperfections couples the clockwise (CW) and counterclockwise (CCW) modes, preventing detection of small rotation rates. Existing solutions typically involve applying a fixed bias rotation using mechanical dithering or non-reciprocal magneto-optic elements to circumvent this limitation.
In this work, the authors propose a new method for biasing RLGs that avoids these traditional approaches. They introduce a self-biasing mechanism based on chiral spontaneous symmetry breaking (SSB) combined with nonlinear frequency pulling in a He-Ne^{20} RLG. This concept allows the system to break the lock-in condition without relying on mechanical bias or external non-reciprocal elements.
The work is original and innovative, and the results are significant. However, there are critical concerns regarding the results that need to be addressed clearly, before any consideration.

Minor issues:
1- Perhaps in all figures authors meant arbitrary units by ‘abr.u.’. Typically, arb.u. or a.u. are used to indicate such units. Authors may need to clarify this.

2-In Figure 4a the unit of Intensity is W. This would need to be clarified whether the vertical axis is power or intensity, or whether the unit is mistyped.

3-In Figure 4a, would the unit of η be Hz/W?

4- Could the author add to the caption or main text, the cause of chirality switch seen in Fig. 3b? Is it a random event or it is a controlled switching via stage rotation?

Major issues:
1- Sagnac Scale Factor Discrepancy: The Fig. 4b presents a significant and critical inconsistency regarding the "Ideal Sagnac response" line, which serves as a crucial theoretical baseline for evaluating the device's performance. The manuscript explicitly states in line 131 that the RLG cavity is a triangle with a 50 mm length with FSR of 2GHz. This dimension is consistent with a Free Spectral Range (FSR) of 2 GHz (FSR=c/L, where L=3×50 mm=0.15 m) for an equilateral triangular cavity. Based on these dimensions and a HeNe laser wavelength of 632.8 nm in line 132 of the main text, the theoretical ideal Sagnac scale factor (4A /(λL)) is calculated to be ~796.2 Hz/(deg/s). This means for a rotation rate of 0.5 deg/s, the ideal Sagnac beat frequency (fs=4AΩ/(λL)) should be approximately 398.1 Hz.
However, Figure 4b explicitly labels the horizontal axis (Ω) in "deg/s" and the vertical axis ("Beat response") in "Hz". When inspecting the "Ideal Sagnac response" line in Figure 4b, it clearly indicates a beat response of approximately 1000 Hz at an angular rotation rate of 0.5 deg/s. This implies a plotted "ideal" scale factor of 2000 Hz/(deg/s).
This creates a critical contradiction: the plotted "Ideal Sagnac response" sensitivity of 2000 Hz/(deg/s) is approximately 2.5 times higher than the theoretical ideal sensitivity of 796.2 Hz/(deg/s) derived from the device's own stated and consistent physical dimensions. This discrepancy cannot be explained by minor factors such as a small shift in operating wavelength

due to detuning (e.g., ~100 MHz) or even by nonlinearity.
Could the authors please address and reconcile this inconsistency?

2- It is recommended the authors add the achiral RLG response to the Fig. 4b in comparison with chiral RLG responses.

3- In Fig. 4b, the 'thumbs-down' data points, observed within the Ω>0 region for the I_CW<I_CCW chiral state, demonstrate a large lock-in threshold. This specific state is attributed in the text to ‘artificial chirality switching,' such as by restarting the power supply. A notable observation is that this artificially induced I_CW<I_CCW chiral state appears to be stably providing a linear beat frequency response.
It is understandable that an I_CW<I_CCW state can be triggered randomly, as the authors mention. However, Fig. 3e illustrates that chirality can also be switched in a controlled manner by rotating the stage. Specifically, rotating the stage in the CW (i.e., Ω>0) direction, even at a rate as small as 0.1∘/s, results in an almost deterministic state of I_CW>I_CCW.
Returning to Fig. 4b, the 'thumbs-down' data for the artificially induced I_CW<I_CCW chirality was obtained under CW rotation at rates Ω>0.2∘/s. Based on the deterministic switching behavior shown in Fig. 3e, one would expect that these data points would not remain stable. Instead, the system should switch back to the 'thumbs-up' data, corresponding to the I_CW>I_CCW chirality, at the same rotation rates (Ω). This expectation is further consistent with the mechanism explained in Fig. 4c, where positive (CW) stage rotation is described as shifting the CW mode towards the gain center (v0), thereby increasing its intensity relative to the CCW mode (i.e., I_CW>I_CCW).
Could the authors please comment on this apparent discrepancy? Specifically, why does the artificially induced I_CW<I_CCW chiral state exhibit such persistent stability in Fig. 4b, and why does it not switch back to the I_CW>I_CCW chiral state when subjected to CW rotation rates that, according to Fig. 3e, should trigger such a transition?

4- The authors state that the RLG's initial state is random upon startup. My understanding is that the process then involves turning on the laser, setting the pump current, and adjusting the laser frequency to a specific set point. However, at this stage, the chiral state may still remain random. Given this, it appears the authors must then rotate the stage or strongly detune the lasing frequency from gain center to deterministically bring the RLG to the desired 'thumb-up' chiral state. Could the authors please confirm if this described initialization sequence is accurate? Furthermore, it is suggested that a detailed explanation of this procedure, specifically how the desired chiral state is reliably set from a random initial state (e.g., confirming the use of stage rotation or other active means), would be highly beneficial if added to the Methods section or Supplementary Information to enhance experimental reproducibility.

5- A few points in Fig. 2:
5-a- I find the horizontal axes in Figs. 2c and 2e confusing. Specifically in Figure 2e, it is not clear whether 'Tuning Frequency' represents a new detuned lasing frequency or detuning from a reference point. To improve clarity and interpretability, I suggest that the authors replot these figures with explicit experimental values on their horizontal axes.

5-b- Additionally, it would be very helpful to add what the shaded regions mean in Fig. 2e. Are they standard deviations of measurements? It can be added to the caption.

5-c- In Fig. 2c what is the operating wavelength of the laser? It can be added to the caption.

5-d- In Fig. 2e what is the applied pump current? It can be added to the caption.

6- Detection Errors on Beat Response: Figure 4b, which presents critical beat note data, notably lacks any indication of measurement uncertainty (e.g., error bars). This contrasts with the inclusion of uncertainty for intensity data in other figures (e.g., Fig. 2c and Fig. 3b).
Quantifying this uncertainty is crucial for a complete assessment of the RLG's high-precision performance, especially given two factors:
A- The method relies on precise sub-100 nm PZT mirror adjustment for bias point setting. Given the stated Zerodur coefficient of thermal expansion (CTE) of <5×10−6 /∘C for the 150 mm cavity e.g., a 0.1∘C temperature fluctuation could induce a cavity length change of ΔL = 75 nm = 0.15m×5×10^(-6)/°C×0.1°C. Such thermal drifts, along with other environmental factors or mechanical movements, could rapidly consume or exceed the available 100 nm adjustment range, directly impacting the frequency offset and introducing noise into the measured beat note.
B- The chiral biasing scheme inherently uses differential intensity (as detailed in Figures 2c and 3b), which may impact beat note signal contrast and thus the precision of its frequency determination.
Could the authors please clarify whether the beat note uncertainties in Figure 4b are really negligible, or alternatively, include error bars for the reported measurements?

7- Robustness of Nanometer-Scale Bias Control in Dynamic Environments: The proposed biasing method effectively eliminates the need for mechanical dithering, which is a significant advantage. However, this technique relies on precise nanometer-scale tuning of a PZT-controlled mirror to set and maintain the laser frequency bias. In practical applications, such as those involving varying operational environments, even minute mechanical noise, thermal fluctuations (leading to thermal expansion/contraction), or other environmental perturbations could induce unintentional cavity length variations of this scale or larger. For example, a thermal drift in the studied RLG can be as high as ~750 nm/ °C, based on the Zerodur CTE provided in Methods. While the stationary Allan plot analysis in Fig. 4d demonstrates excellent stability, possibly in a controlled and static environment, it does not fully capture performance under dynamic or perturbed conditions. It would be highly beneficial to explicitly address the potential impact of these external factors on the stability and performance of the chiral RLG, and comment on strategies for mitigating such effects if any.

Referee #2

(Remarks to the Author)
Manuscript ID: AE12826

Title: Chiral laser gyroscopes breaking the lock-in limit

Authors: by Yuan-Hao Mao, Ji-Peng Xu, Hong-Teng Ji, et al.

Anamnesis:

The manuscript's main result is the experimental proof that a ring-laser-gyroscope (RLG) can operate at very low rotational speed, lasing on a single He-Ne^{20} isotope. Usually, these devices in this configuration cannot measure low rotational speed due to the mode lock-in phenomenon that prevents setting a frequency difference among the two counter-propagating modes in an active Sagnac interferometer. The experimental proof is complemented by a detailed theoretical analysis of the system and some numerical simulations.

The abstract introduces the self-locking problem affecting RLGs at low rotation rates and the reported solution. The main text then starts with a nod to RLG's history, then focuses on the locking issue and the approaches adopted so far to overcome it. Before entering the core of their work, the authors recap chiral systems in optics and their potential applications.

The manuscript core is essentially divided into two parts. The first concerns the asymmetric behaviour (chirality) of the ring laser cavity, the second discusses its impact on the performance of the chiral singleisotope RLG at low rotation rates.

Main comments

The paper results are surely novel and scientifically sound. They may be of interest to a pretty large audience, spanning physicists, engineers and more generally navigation experts. The main claim, which, after reading the paper twice, became clear, is the possibility of employing an RLG at low rotation rates. However, some shortcomings deserve consideration:

1. The most important, in our opinion, is the possibility of controlling the proportionality factor, also known as the scale factor, between the rotation rate and the Sagnac frequency in a replicable, reliable and sufficiently precise manner. This implies including in the manuscript a detailed description of the relation among cavity detuning, RLG working point (e.g. pump power and gas pressure) and the non-linear parameter $\xi\xi$. The interplay between these experimental quantities is evident all over the paper, but an explicit, auto-consistent analysis is missed. This absence prevents the possibility of a complete evaluation of the replicability and the sensitivity of the system. We refer to: a) the connection (Fig.1f) between non-linear coupling and frequency separation and the ratio between the intensities of CW and CCW beams; b) the relation between α (net gain coefficient) and pump current (Fig.2c-d); c) the relation between $\xi\xi$ and tuning frequency (Fig. 2d-e). All these experimental figures play a role in fixing the frequency bias, which in Fig. 4a is reported as a function of the detuning from the centre of the laser frequency, so that a much more clearer analysis of their interplay is necessary both from the theoretical and experimental point of views to support the effectiveness of the proposed method in terms of replicability. Moreover, the sensitivity of the instrument is never assessed with respect to a change in the working conditions. What will happen to it if the pump power has a 5% stability in 1 hour? What happens if the cavity resonance drifts for some reason?

2. The second shortcoming regards the SSB regime. From Eq. (3) is clear that a change in the sign of (IIcw – IIccw) affects the measured frequency difference, thus making the instrument unreliable if this sign is assigned randomly at the switching on of the instrument. It is not clear, from the actual text, if the authors suggest circumventing this by systematically using the second analysed method, “rotation-induced controllable chirality,” or if the two methods can be used interchangeably and other “tricks” can be used. In the former case, if we got it right, the claim that the presented system does not require external components would fail, as it would include a rotation stage.

3. A third one regards the instrument SNR. The unbalancing of the two beams inherently reduces the fringe contrast of the Sagnac signal. This leads to a reduction in the SNR of the instrument and then its precision. A discussion on the accuracy of the instrument and, in particular, on the effect of the intensity unbalance on it is an important issue that is missing in the text.

4. In addition, to justify a non-vanishing steady-state value of (IIcw – IIccw) in Eq. (3) for the frequency shift, the authors study the evolution of the intensities towards their stationary values in the section “Spontaneous chiral symmetry breaking.” The analysis is based on Eq. (1) in the main manuscript, or more precisely, Eq. (S1) in the Supplementary Material. In these equations, contrary to what happens in the cited references and in standard RLG models (e.g. the review of Wilkinson 1987 https://doi.org/10.1016/0079-6727(87)90003-6), the evolution of the intensities looks uncoupled from the phases. This approach, not explicitly mentioned in the text, requires a clear justification. Moreover, it is unclear how the connection between IIcw – IIccw and the phase difference appears in Eq. (3) (see comment 2) if the two dynamics are completely uncoupled.

Textual comments

a. Line 22: The authors use "chiral spontaneous symmetry breaking" for the physical phenomenon underlying the whole manuscript, while at line 74, they use "spontaneous chiral symmetry breaking". We suggest using the same terminology throughout the paper.

b. Line 32: We suggest including more references on RLGs in Fundamental Physics experiments. A tentative, quite recent list can be extracted from https://doi.org/10.3389/frqst.2024.1363409.

c. Line 36: The references cited here (6-8) are not adequate in this context if the intent is to introduce the Sagnac effect to the general public, since none of those papers is a seminal work on the Sagnac effect. A general audience would benefit from a more pictorial explanation of the Sagnac effect and, possibly, citing some seminal and review papers (e.g. Wilkinson 1987 https://doi.org/10.1016/00796727(87)90003-6 is a review that starts with a historical part). References 6-8 should be moved elsewhere in the paper if appropriate.

d. Lines 41-43: Appropriate citations should be added for the two mentioned methods.

e. Line 45: We suggest moving the references to the end of the sentence.

f. Lines 49-51, 69, 70: The concept of chiral for intensities, as far as we know, appears in Ref. 32, while in all the other cited papers, the term “chiral” is used in different contexts. We suggest stressing this point to avoid confusion in a non-specialised reader.

g. Lines 84-85, eq. (1): Eq (1) where field amplitudes appear as independent from the corresponding phases, contradicts the standard model for RLG (e.g. Ref. 38, cf. eq.. 2.3 and 2.4 in the dissipative case). Moreover, Eq. (1) can’t be interpreted as a special case of Eq. (2.3) in Ref. 38 without assuming either a constant phase difference or r=0 (trivial case). If Eq. (1) is to be intended as an intentional deviation from the well-established models, we suggest motivating it and explicitly addressing it in the text. Eventually, we suggest specifying that the parameters in Eq. (1) are real constants.

h. Lines 95-105 (caption of fig. 2): units are missing everywhere (even if the field amplitudes are dimensionless, the parameter \alpha and r still have units of the inverse of the time). Why the value of r is never specified? Are the bifurcating surfaces and curves in Fig. 1.a,b,d showing the steady state intensity solutions of Eq. (1)? Are the simulations in Fig. 1.f-I too based on Eq. (1)? If yes, we suggest clarifying considering also the above comment (g.). Even if the experimental data shown in Figs. 2.e and 2.f qualitatively seem to follow the simulations in Figs. 2.b and 2.d, the scale chosen for the axis doesn’t allow for appreciating whether the agreement is also quantitative.

i. Lines 114-119: It is not clear how \alpha and \xi are related to the pump current and the tuning frequency, respectively (see main comment 1.).

j. Lines 119-120: The evolutions in Fig. 2g and 2i are reported in time, but it is not clear if this is just the RLG running time since the switching on of the pump, or if, during that time, there is a tuning of some experimental parameters. Please clarify.

k. Lines 125.126: “Remarkably, as shown in Fig. 2i, a mere 0.1% initial intensity…” The scale adopted in Fig. 2i does not allow for seeing the initial imbalance. Either rephrase or add an inset to the figure.

l. Lines 136-142 (caption): colour scheme of Fig. 3e and 3f, and percentages in Fig. 3f are potentially misleading. We suggest using the same colours for the graphs and the arrows associated with the same rotation orientation. The matrix representation in Fig. 3f is not clear at first. We suggest specifying in the caption that in Figs. 3d and 3f, the modes with higher intensity are counted at each run.

m. Line 144-146: A “control paradigm” based on randomness is, in our view, a contradiction.

n. Lines 155-156: The authors experimentally proved that in the SSB phase, there is a correlation between the direction of rotation of the RLG and the orientation of the mode with the highest stationary intensity. However, if field intensities are decoupled from the rotation in the theoretical model (cf. Eq. (1)), it is not clear how this can happen (see main comments 2. and 4.).

o. Line 162: For the sake of clarity, a text comment, possibly with cross references, should address how Eqs. (2) and (3) are related to Eq. (1) and Eq. (S1) in the Supplementary Material. \ni is not defined. It is not clear how \Delta\ni is related to the phase difference and to Eq. (S2) in the Supplementary Material.

p. Lines 193-197: Please improve the discussion of on Fig. 4b to help the reader in a full understanding of the different experimental curves, especially because the curves appear as connected and having the same colour in the plots.

q. Lines 241-242: “… promising transformative impacts across metrology, integrated photonics, and quantum precision measurement systems”. This sentence is too generic if not supported by references.

r. Eq. (S1) in the Supplementary Material: General comment 4. applies. Moreover, the phases are real functions of time, so the last two equations in Eq. (S1) are inconsistent for values of r different from zero.

s. Text before Eq. (S2) in the Supplementary Material: please give an estimation for the back-scattering ratio r to justify the assumption of a small quantity.

t. Eqs. (S3)-(S7) are obtained from Ref. 4-6. It would be of help to reference also where (page/section/Eqs) in the cited papers this model is given.

Eventually, the data complementing the manuscript are not of immediate use. Data for Fig. 2: i) the legend is missing, data cannot be easily interpreted; ii) file coupling: no indications on how the error bars are constructed, the legend is not clear; in particular, if the first column represents the pump current, why are its units “s”? iii) Data for Fig. 3b: why are the data on the x-axis in Fig. 3 b reported with units of mA, and in the table, they have units of s?

Final Recommendation

We believe that the actual manuscript can possibly be re-evaluated for publication in Nature, or in a more specific journal of the Nature group, after all the main shortcomings are completely solved.

Referee #3

(Remarks to the Author)
I co-reviewed this manuscript with one of the reviewers who provided the listed reports.

Referee #4

(Remarks to the Author)
This paper proposes to solve the inherent lock-in effect in ring laser gyroscopes (RLGs) through spontaneous symmetry breaking (SSB) without requiring mechanical dithering or magneto-optic biasing elements. This represents a major innovation in traditional RLG design paradigms. With solid theoretical foundations and sufficient experimental data, it constitutes an excellent gyroscope-related paper.
I have the following comments for this manuscript:
1. The physical meaning of the nonlinear coupling coefficient ξ needs clarification in the main text, as it currently only appears in the appendix.
2. The physical mechanism of the nonlinear frequency pulling term η(Icw−Iccw) in Equation (3) Δv=([η(Icw−Iccw)+ΔvS]2−4r2)1/2 requires supplemental explanation.
3. The abstract mentions this method would significantly advance all-solid-state laser gyroscopes, but the implementation is based on He-Ne lasers. Are the theoretical derivations universally applicable? Similarly, can this theory be extended to fiber-optic gyroscopes or silicon-based microresonator gyros? This point should be rigorously discussed to attract broad interests to the laser gyroscope community.
4. Supplement discussion on challenges for solid-state implementation in experiments and potential solutions.
5. The main text repeatedly uses "deg/h" while Figure 4d uses "°/h". The manuscript should standardize angular unit notation.
6. High-intensity mode competition may cause local thermal lensing effects, but the text doesn't discuss temperature drift impacts on cavity length stability. Was temperature control implemented during actual experiments?
7. What is the stability limitation in Fig.4(d)? How can it be improved in the future?

Version 1:

Reviewer comments:

Referee #1

(Remarks to the Author)
I thank all the authors for their careful and thorough responses to the reviewers’ comments. Excellent work! I believe the concerns have been successfully addressed, and the manuscript is a perfect fit for Nature.

Referee #2

(Remarks to the Author)
General comment

The manuscript has undergone significant revisions following the first round of reviewers. However, some of the major issues we previously raised remain unresolved. We also compared our comments with the ones raised by the other referee, finding more than one point of contact.

Carefully reading all the submission material and cross-checking among the different versions, including the Supplemental Material, the newly added sections in the methods, and, in particular, the coherence among simulations, theoretical model and relative plots, and experimental findings, we identified some inconsistencies in detail that prevent the manuscript from being accepted for publication in Nature.

The developed model of the RLG is not completely consistent with the reported experimental parameters. The latter are treated in a very qualitative manner, preventing the reader from understanding how the simulations, the analytical model, and the experimental features can be viewed under a unified framework. For details on our perspective, please read items 1.b, 2, 3, and 4 below.

The inconsistency found by the other referee regarding the geometrical factor and the reported construction parameters in the first version raises a serious concern about the accuracy in preparing the entire manuscript. In the first report, we didn't go into too many details on some of the "main comments" we raised. We regret to say that the authors missed to solve some of them leaving the level of discussion too qualitative. We have tried to evidence in the following the most critical points.

Here is a list of detailed comments (numbers and letters refer to our comment, main and textual, original lists and the relative authors' reply):

Comments to replies to main comments

1. We asked to include "in the manuscript a detailed description of the relation among cavity detuning, RLG working point (e.g. pump power and gas pressure) and the non-linear parameter $\xi\xi$. The interplay between these experimental quantities is evident all over the paper, but an explicit, auto-consistent analysis is missed."; Referring to
a. the connection (Fig.1f) between non-linear coupling and frequency separation and the ratio between the intensities of CW and CCW beams;
b. the relation between α (net gain coefficient) and pump current (Fig.2c-d); c) the relation between $\xi\,\xi$ and tuning frequency (Fig. 2d-e).

a. We understand that Fig. 1f represents a behaviour and not an analytical plot, but citing Eq.(4) does not give an idea of the assessed linear dependence between the frequency splitting and the intensity difference. In addition, the equation for \eta, given in the reply to our comment, should have been inserted in the manuscript.

b. Fig.2 shows several issues. First, to correctly compare the simulations with the experimental data, the plots need to have the same parameters on both axes and the same scales. How can the reader compare the scale of \alpha, given in Hz, with the pump current, given in mA? How can we compare different vertical scaling? How can the reader convert $\xi\xi$, that is adimensional, into Hz? If in c and e the intensity is a measured one, it cannot be in arb.u.! The caption reports that plot b has been obtained by setting $\xi\xi$ =1.09, while plot d refers to $\alpha\alpha$ = 1200 Hz. If so, the graphs are not consistent! The intensity difference at $\alpha\alpha$ = 1200 Hz in b is roughly 3 (black line just below 4, red one below 1), while at $\xi\xi$ = 1.09 in d the difference looks more than 5 (black line close to 6, red one well below 1).
The text reports that $\alpha\alpha$ and the pump current are proportional. From the caption, one reads that 1200 Hz corresponds to 0.6 mA, but at 0.6 mA in c, the red curve is higher than the red curve in b at 1200 Hz. Moreover, the bifurcation in b happens around 700 Hz; if the two quantities are truly proportional in the plotted range, the bifurcation should appear, in c, around 0.37 mA and not close to 0.5 mA, where it is now. By the way, the symbol vv, pedex free, appears in the caption of Fig.2 for the first time, and then in the caption of Fig.4, while it is defined in the text at line 221, if they are the same quantity.

2. There is still some missing information to understand the physics of the system. In particular, from the graph in Fig. S5c, it can be inferred that the system is intrinsically asymmetric. A higher intensity of the CW beams looks like a preferred state. Where does this feature come from? The scheme shows two additional laser sources coupled to both propagation directions. It is unclear why feedback is provided and/or required on both beams.

3. We asked to include in the manuscript a discussion on the effect of the intensity unbalance on fringe contrast and the SNR of the instrument (see Comment 3). The authors address the point in their reply, but it is not included in the actual manuscript. By the way, in their reply the authors use unprecise values for the output powers of the beams: as can be seen in Fig. 4a, at the operating point $vv3$ ("the point of maximum frequency bias") the output powers of the CW and CCW beams are slightly less than 6μW and slightly higher than 2μW respectively, and not approximately 5μW and 3μW as reported by the authors. Moreover, while for 5μW and 3μW is correct that the beat note amplitude would reduce by 3.2%, the reported formula is wrong the correct one being �$II1II2$. The beat note amplitude for the correct powers at "the point of maximum frequency bias", then, reduces by more than 10%.

4. The authors amended the laser equations in the Supplementary Material and in the Methods section only. These amended equations are not used in the actual version of the main text. In particular, the new set of coupled equations (S1)-(S3) predicts Eq. (S8) for the instantaneous frequency, but Eq. (S8) is never used in the main text. On the contrary, the theoretical model in the main text is still based on Eq. (3). The link between Eq. (3) and Eq. (S8) is not clear, since they exhibit exact agreement in the achiral case only (i.e. same intensities) and not in the much more interesting achiral case that is the focus of the regime actually investigated. Moreover, it is not clear what the authors mean by "steady-state chiral solutions to the amplitude equations (S2)" just before Eq. (S4). Do the authors mean that the equations (S2) admit exact or approximate steady-state solutions for the intensities?

Comments to reply to textual comments:

h. We asked the authors to clarify the units used for the plots in Fig. 2. In their reply to our comment, the authors write: "Based on the comparison with our experimental data (Fig. 4b), we determined that the backscattering coupling coefficient r is approximately 30 Hz. Consequently, all linear frequency parameters in our model required scaling. Specifically, the linear gain coefficient $\alpha\alpha$ has also been scaled to maintain consistency with the physical system." It is not clear what the authors mean, given that the new horizontal axis for the plot in Fig. 2b has been rescaled by a factor of 1500 Hz compared to the previous version. Moreover, in the same response, the authors say: "The theoretical plots in Fig. 2 are now based on Eq. (4) in the Methods section, which is derived from Eq. (1) using the separation of variables method for the amplitude equations." However, apart from the already discussed rescaling of the horizontal axis, there are no visible differences between the theoretical plots in Fig. 2 in the present version of the manuscript and the previous one. This comment is very much related to the main comment 1-b given above.

j. In response to our Comment #j the authors say that in Fig. 2g and 2i the horizontal axes "does not represent the physical running time of the RLG but rather the convergence time of the numerical solution. To avoid misunderstanding, we have modified the labels on the horizontal axes in Figs.2g and 2i, accordingly." The authors should explicitly state in the caption of Fig. 2 that the plots f-i are simulations. Moreover, the units and ticks on the horizontal axes should be reintroduced. The use of arb.u. for intensities is not convincing, especially because the numbers mimic actual values in µW as it appears from the authors' reply to main comment 3.

o. The equation for the beat frequency Δv in the authors' reply to our comment #o should be included in the manuscript. Moreover, the choice of integration time T should be clarified.

s. In Comment #s we asked to provide "an estimation for the back-scattering ratio r to justify the assumption of a small quantity." Even if in their reply to our comment, the authors say that "In the revised derivation, it is no longer necessary to approximate or ignore the backscattering coefficient r", the manuscript would benefit from the inclusion of an estimate for the backscattering coefficient. Note that the value reported in the reply (30 Hz) is not included in the manuscript. Moreover, "smallness" of r can be assessed only when compared to the (rotation-dependent) Sagnac frequency \Omega_S. To facilitate the comparison, we suggest including an estimate of the scale factor S and/or typical values of \Omega_S for relevant values of rotation.

Moreover, the data complementing the manuscript are still not of immediate use. In particular, the authors say in their reply: "The data file named "e-increasing coupling.CSV" for Fig. 2e records the optical intensity variation under continuous linear frequency tuning. This data was acquired directly from an oscilloscope; therefore, the first column represents the time (in seconds) recorded by the oscilloscope, which corresponds to the frequency shift during the continuous tuning process." Note that this discussion is not included in the text and should be added. By the way, without an indication of the constant rate of the frequency tuning, it is not possible to relate the "scanning time" to the values of the frequency on the horizontal axis of Fig. 2e. Moreover, in all the files, units for the intensities are missing or are different from the ones reported in the actual plot. For example, in the data for Fig. 2 the units for the intensities are missing and the values are not in the range showed on the vertical axis of the plots in Fig. 2c and 2e.

New comments in view of the amended text

1. At line 179, the frequency \Omega_S is introduced. The link with \nu_S introduced at line 37 is not clear.
2. At lines 96-97 of the manuscript, the authors say that: "$\alpha\alpha$ is proportional to the pump current within the gain range (0.4~0.8 mA) studied in this work". However, as can be clearly seen from Fig. 2c just below the experimental data range is larger (at least 0.2-0.8 mA). Moreover, where is it possible to see the proportionality between $\alpha\alpha$ and the pump current? See the comment to Fig. 2 above for the proportionality issue.
3. At line 141, we suggest specifying whether 125 mm is the cavity side length or the total length.
4. At line 176, it is not clear what the authors mean by "approximate gain clamping condition" used to derive Eq. (2). Moreover, for self-consistency, the authors should add how this approximation is implemented in relation to the equations in the Supplementary Material (Eqs. (S1)-(S8)).
5. Eq. (3) is not consistent with Eq. (S8) (see also below comment 10).
6. Throughout the text, the symbol $\nu\nu$ is used, but its definition is not clear. In the main text, the frequency $\nu\nu$ is mentioned for the first time at line 221 as "the operating frequency of the RLG". It is not entirely clear what this actually indicates, and whether there is a connection to the resonance frequency of the ring cavity, ω, which is defined at line 87.
7. At line 278, the authors provide information on the stability for a cavity of length 0.375m, but the actual cavity length is 125 mm (line 141). Thus, the information provided by the authors may be misleading regarding the actual RLG geometry.
8. After line 299, it is not clear why they need to introduce the functions f and g. As far as it is possible to follow the reasoning underneath, the two coincide with the expressions given in Eq. (4) unless there are unexpressed approximations apart from cosΔu =1. If so, please specify the approximate expression used for f and g.
9. In Eq. (S8) the definition of the mean < > should be provided (see Comment #o). The link between Eqs. (S8) and (3) is not clear since they are consistent in the achiral case only. The discrepancy between the two methods in the chiral case should be quantified with reference to the actual data range studied in the manuscript.
10. Fig. S4a is not consistent with Fig. 2d (compare the values of the intensities in the two plots for \alpha=1200 Hz and \xi=1.07). By the way, the authors should explicitly state in the caption of Fig. S4 that the plots are simulations.
11. In the Section. "Frequency stabilization method", when the authors say "its derivative, the discrimination signal D(v)", we suggest to specify that it is the derivative with respect to time.

Referee #3

(Remarks to the Author)
I co-reviewed this manuscript with one of the reviewers who provided the listed reports.

Referee #4

(Remarks to the Author)
The author has answered all my questions. I am satisfied with these responses and have no further questions.

Version 2:

Reviewer comments:

Referee #2

(Remarks to the Author)
Manuscript ID: AE12826
Title: Chiral laser gyroscopes breaking the lock-in limit
Authors: by Yuan-Hao Mao, Ji-Peng Xu, Hong-Teng Ji, et al.
General comment
The authors have solved most of the critical issues we have identified in our second report.
However, we underline a possible small inconsistency that may require a further authors' check.
the definition of $\Omega_S$at line 37 may not be consistent with the use in Eq. (4) a factor ½ looks missing. Using the present formulas the frequency difference would be $〖2\Omega〗_S$.
We agree that the presented results are of wide interest for future application and studies on RLG and can be published, in the present form, in Nature.

Referee #3

(Remarks to the Author)
I co-reviewed this manuscript with one of the reviewers who provided the listed reports.

Responses to the comments of Referee #1

Referee #1:

The manuscript 'Chiral Laser Gyroscopes Breaking the Lock-in Limit' presents an interesting approach to overcoming one of the longstanding challenges in ring laser gyroscopes (RLGs): the lock-in phenomenon. In conventional RLGs, backscattering from mirror imperfections couples the clockwise (CW) and counterclockwise (CCW) modes, preventing detection of small rotation rates. Existing solutions typically involve applying a fixed bias rotation using mechanical dithering or non-reciprocal magneto-optic elements to circumvent this limitation. In this work, the authors propose a new method for biasing RLGs that avoids these traditional approaches. They introduce a self-biasing mechanism based on chiral spontaneous symmetry breaking (SSB) combined with nonlinear frequency pulling in a He-Ne^{20} RLG. This concept allows the system to break the lock-in condition without relying on mechanical bias or external non-reciprocal elements. ***The work is original and innovative, and the results are significant.*** However, there are critical concerns regarding the results that need to be addressed clearly, before any consideration.

Response:

Thank you for your thoughtful and positive assessment of our work, and for recognizing its originality and significance in addressing the longstanding lock-in challenge in ring laser gyroscopes. We are particularly grateful for the reviewer's insightful comments and the critical concerns they have raised.

We agree with the reviewer that addressing these points would improve our manuscript. In the following pages, we have provided a comprehensive, point-by-point response to each of the specific comments. We have also performed additional experiments, theoretical analyses, and numerical simulations as suggested, which have substantially strengthened our results and clarified the presentation.

Minor issues:

1- Perhaps in all figures authors meant arbitrary units by 'abr.u.'. Typically, arb.u. or a.u. are used to indicate such units. Authors may need to clarify this.

2- In Figure 4a the unit of Intensity is W. This would need to be clarified whether the vertical axis is power or intensity, or whether the unit is mistyped.

3- In Figure 4a, would the unit of η be Hz/W?

4- Could the author add to the caption or main text, the cause of chirality switch seen in Fig. 3b? Is it a random event or it is a controlled switching via stage rotation?

Responses to minor issues:

We sincerely thank the reviewer for their attentive review and constructive comments, which have helped improve our manuscript. We have addressed each point raised as detailed below.

1. We thank the reviewer for pointing this out. We have replaced “abr.u.” with the standard notation “arb. u.” (arbitrary units) in all figures for clarity.

2. We thank the reviewer for this thoughtful comment regarding the units in Figure 4a. The values labeled "Intensity" on the vertical axis were originally recorded as dimensionless signals from our photodetector, rather than being directly measured with a power meter. To enhance the rigor and clarity of our presentation, we have calibrated the photodetector's response and established a conversion relationship: an output intensity of 0.1 corresponds to an optical power of 2 μW. We also replace the 'Intensity' by 'Power' of the vertical axis. The figure has been updated accordingly to reflect this calibration. We appreciate the opportunity to clarify this point.
3. This is a valid point. The unit of η is Hz/W and it has been modified according to the calibration mentioned above.
4. We appreciate this question. The chirality switch observed in Fig. 3**b** occurred under stationary conditions (no rotation). At that time, the system exhibited bistability, meaning both chiral states can exist. A slight disturbance (e.g., a sudden vibration to the platform) was sufficient to trigger the chiral switch shown. We have added a note in the main text to clarify this point.

All these modifications have been incorporated into the revised manuscript.

Major issues:

Comment #1. Sagnac Scale Factor Discrepancy: The Fig. 4b presents a significant and critical inconsistency regarding the "Ideal Sagnac response" line, which serves as a crucial theoretical baseline for evaluating the device's performance. The manuscript explicitly states in line 131 that the RLG cavity is a triangle with a 50 mm length with FSR of 2GHz. This dimension is consistent with a Free Spectral Range (FSR) of 2 GHz (FSR=c/L, where L=3×50 mm=0.15 m) for an equilateral triangular cavity. Based on these dimensions and a HeNe laser wavelength of 632.8 nm in line 132 of the main text, the theoretical ideal Sagnac scale factor (4A/(λL)) is calculated to be ~796.2 Hz/(deg/s). This means for a rotation rate of 0.5 deg/s, the ideal Sagnac beat frequency (fs=4AΩ/(λL)) should be approximately 398.1 Hz. However, Figure 4b explicitly labels the horizontal axis (Ω) in "deg/s" and the vertical axis ("Beat response") in "Hz". When inspecting the "Ideal Sagnac response" line in Figure 4b, it clearly indicates a beat response of approximately 1000 Hz at an angular rotation rate of 0.5 deg/s. This implies a plotted "ideal" scale factor of 2000 Hz/(deg/s). This creates a critical contradiction: the plotted "Ideal Sagnac response" sensitivity of 2000 Hz/(deg/s) is approximately theoretical ideal sensitivity of 796.2 Hz/(deg/s) derived from the device's own stated and consistent physical dimensions. This discrepancy cannot be explained by minor factors such as a small shift in operating wavelength due to detuning (e.g., ~100 MHz) or even by nonlinearity.

Could the authors please address and reconcile this inconsistency?

Responses #1:

We are extremely grateful to the reviewer for their thorough scrutiny and for identifying this significant discrepancy. The calculation is entirely correct based on the parameters (50 mm side length, 2 GHz FSR) provided in the original manuscript.

This inconsistency arose because we inadvertently cited the parameters from an earlier prototype device (50 mm side length) used in preliminary feasibility studies, while all experimental data presented in Fig. 4**b** were obtained from the actual device batch (125 mm side length) used for the final performance validation.

The correct side length of the ring laser gyro (RLG) cavity used for the results in Fig. 4b is 125 mm. For an equilateral triangular cavity, the total optical path length L is 0.375 m, whose corresponding free spectral range (FSR) is 800 MHz. Using the He-Ne laser wavelength (λ = 632.8 nm) and the formula for the Sagnac scale factor ($S = 4A/(\lambda L)$), where A is the area enclosed by the triangular cavity, the theoretical ideal scale factor is recalculated to be ~1990.5 Hz/(deg/s). Consequently, at a rotation rate of 0.5 deg/s, the ideal beat frequency should be ~995.3 Hz.

Revision: We have thoroughly revised the manuscript to reflect the correct parameters (125 mm side length, 800 MHz FSR) throughout the text (including lines 140-143, page 7, and any other relevant sections).

"As shown in Fig. 3**a**, to experimentally study the chiral SSB phase in a two-frequency RLG (i.e., only a single longitudinal mode oscillates in both CW and CCW directions), we fabricated a triangular He-Ne[20] RLG with a length of 125 mm. Its cavity supports a free spectral range of 800 MHz at 632.8 nm and is mounted horizontally on a rotation stage."

<u>Comment #2</u> It is recommended the authors add the achiral RLG response to the Fig. 4b in comparison with chiral RLG responses.

<u>Response #2:</u>

Thank you for raising this point regarding the achiral RLG responses.

To address this, we have performed new experiments. Specifically, we systematically tuned the laser frequency (shifting the operating point to ν_a) while maintaining constant gain, thereby driving the system into the achiral state for signal response measurement.

The corresponding experimental data and theoretical calculations have now been included in the revised Fig. 4b.

Revision:

We have added the achiral RLG response to the revised manuscript. (lines 211-213, page 11)

"…In contrast, when the operating point is tuned to ν_a as shown in Fig. 4**a**, the gyroscope operating in the normal achiral state exhibits a nonlinear frequency response at a rotation speed below 0.05 deg/s and enters the lock-in region when $\Omega < 0.03$ deg/s…"

Due to the relatively small lock-in threshold of the RLG used in our work, the experiment data in the achiral state closely approximates the ideal response.

As a result, we have removed the former "Ideal Sagnac response" line from Fig. 4b to avoid redundancy and potential confusion. In addition, the caption of Fig. 4b is also revised.

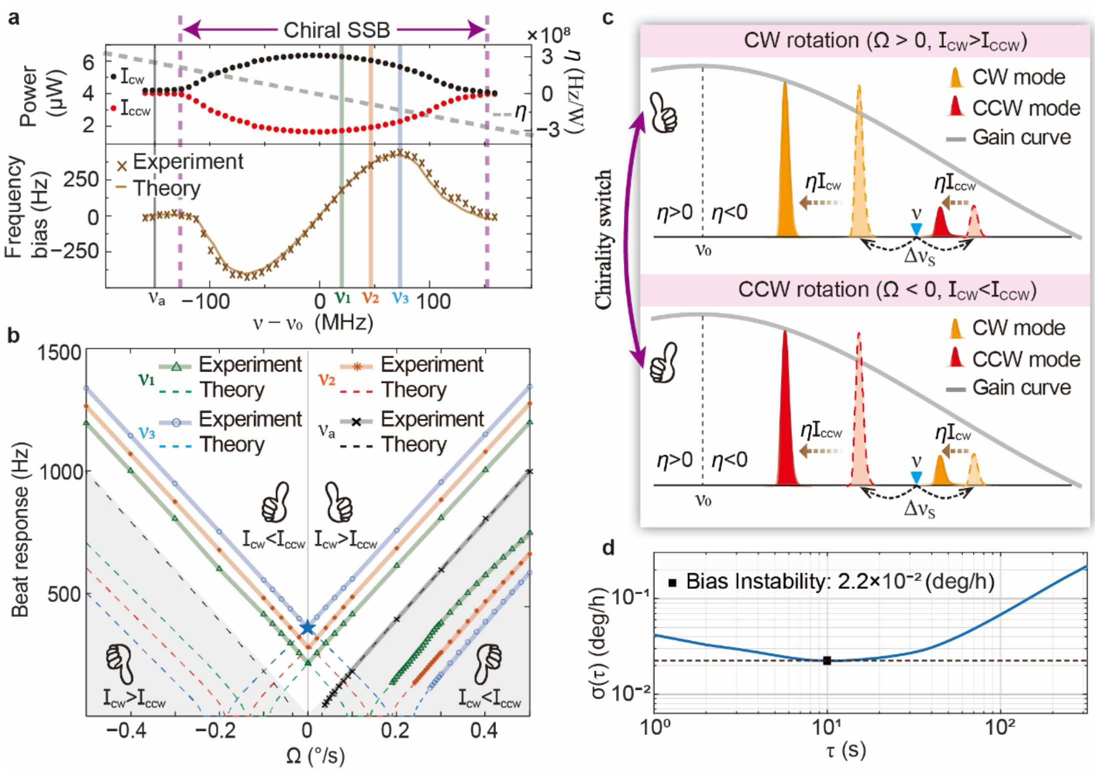

Fig. 4| Frequency response characteristics of the RLG in the chiral SSB phase. a, (upper panel) The CW/CCW mode intensity, nonlinear frequency pulling coefficients η and (lower panel) the corresponding frequency bias with tuning frequency ν around the Ne^{20} gain center ν_0. **b,** The frequency response to low rotational speed of the RLG under different operating points and chirality states. ν_1, ν_2, ν_3 denote the chiral states and ν_a corresponds to the achiral state. **c,** Schematic of chirality switch and frequency bias principles for the RLG under CW/CCW rotation conditions. Ω_S is the frequency shift caused by Sagnac effect. **d,** Allan variance analysis of 1000-second frequency bias stability test at the operating point indicated by the blue star in **b**.

Comment #3- In Fig. 4b, the 'thumbs-down' data points, observed within the Ω>0 region for the ICW<ICCW chiral state, demonstrate a large lock-in threshold. This specific state is attributed in the text to 'artificial chirality switching,' such as by restarting the power supply.

A notable observation is that this artificially induced ICW<ICCW chiral state appears to be stably providing a linear beat frequency response.

It is understandable that an ICW) direction, even at a rate as small as 0.1°/s, results in an almost deterministic state of ICW > ICCW.

Returning to Fig. 4b, the 'thumbs-down' data for the artificially induced ICW 0.2°/s. Based on the deterministic switching behavior shown in Fig. 3e, one would expect that these data points would not remain stable. Instead, the system should switch back to the 'thumbs-up' data, corresponding to the ICW > ICCW chirality, at the same rotation rates (Ω). This expectation is further consistent with the mechanism explained in Fig. 4c, where positive (CW) stage rotation is described as shifting the CW mode towards the gain center (v0), thereby increasing its intensity relative to the CCW mode (i.e., $I_{CW} > I_{CCW}$). Could the authors please comment on this apparent discrepancy? Specifically, why does the artificially induced $I_{CW} < I_{CCW}$ chiral state when subjected to CW rotation rates that, according to Fig. 3e, should trigger such a transition?

Responses #3:

We appreciate your thoughtful analysis of our work. Analyzing these questions allowed us to refine our argument and has led to a much clearer presentation in the revised manuscript. We would like to clarify the experiment results in the "thumbs-down" region with following points:

1. **Dual-potential-well structure and metastability**
   As detailed in **Supplementary Material S3**, when the system operates in the chiral state, it exhibits a dual-potential-well structure, corresponding to the two stable states represented by the "thumbs-up" and "thumbs-down" regions in Fig. 4**b**. By repeatedly restarting the power supply, it is possible to stabilize the system in the "thumbs-down" chiral state. As you anticipated, this state is indeed metastable under clockwise rotation ($\Omega > 0$) and tends to transition toward the more stable "thumbs-up" state ($I_{CW} > I_{CCW}$). However, our experimental results indicate that the timescale required for this transition is sufficiently long to allow stable measurement of the beat frequency response in the "thumbs-down" state. This metastability is consistent with the energy barrier between the two potential wells, which slows down the transition process.
2. **Chirality control via seed light injection**
   According to the theoretical framework presented in our manuscript, the steady-state intensities of the clockwise (CW) and counterclockwise (CCW) laser modes depend on their initial values. Therefore, we injected seed light into the CCW mode during the experiment to enhance the stability of the system in the "thumbs-down" state ($I_{CW} < I_{CCW}$) under external rotation. This approach, illustrated in Figs. S5**a** and S5**b** of the Supplementary Material (for which we have a patent application in process), can also effectively bias the system toward the desired chiral state during the initialization startup of the chiral RLG.
3. **Purpose of artificially inducing $I_{CW} < I_{CCW}$ state**
   The primary purpose of artificially inducing and characterizing the $I_{CW} < I_{CCW}$ chiral state under clockwise rotation was to comprehensively discuss the frequency bias under different chiral states. By demonstrating the beat frequency response in both chiral states, we aim to provide a more complete understanding of how chiral output influences the frequency bias in laser gyroscopes. This approach allows us to explore the different behaviors predicted by our theoretical model.

We hope that this clarification addresses your concerns regarding the discrepancy. Our results highlight the rich dynamics and metastable properties of the system, which are integral to the chiral switching mechanism.

Revision: We have added related discussion in the main text to clarify this discrepancy (Lines 213-219, page 11):

"Notably, a chirality flip occurs concurrently with the reversal of the rotation direction, which is consistent with the experimental results presented in Fig. 3**e**. Furthermore, to comprehensively validate the effect of chirality on the frequency bias, the chirality is artificially switched (such as restarting the power supply with a directional seed light) during clockwise rotation. As indicated by the "thumbs-down" region in Fig. 4**b**, this chirality-switched state produces a significant negative frequency bias, which in turn substantially increases the lock-in threshold of the RLG.**”**

Comment #4 The authors state that the RLG's initial state is random upon startup. My understanding is that the process then involves turning on the laser, setting the pump current, and adjusting the laser frequency to a specific set point. However, at this stage, the chiral state may still remain random. Given this, it appears the authors must then rotate the stage or strongly detune the lasing frequency from gain center to deterministically bring the RLG to the desired 'thumb-up' chiral state. Could the authors please confirm if this described initialization sequence is accurate? Furthermore, it is suggested that a detailed explanation of this procedure, specifically how the desired chiral state is reliably set from a random initial state (e.g., confirming the use of stage rotation or other active means), would be highly beneficial if added to the Methods section or Supplementary Information to enhance experimental reproducibility.

Responses #4:

We appreciate your insightful observation regarding the initialization process of the RLG and the experimental steps taken to achieve a deterministic chiral state. To elaborate this issue, we have added a new Figure S5 in the **Suppelementary Materials**.

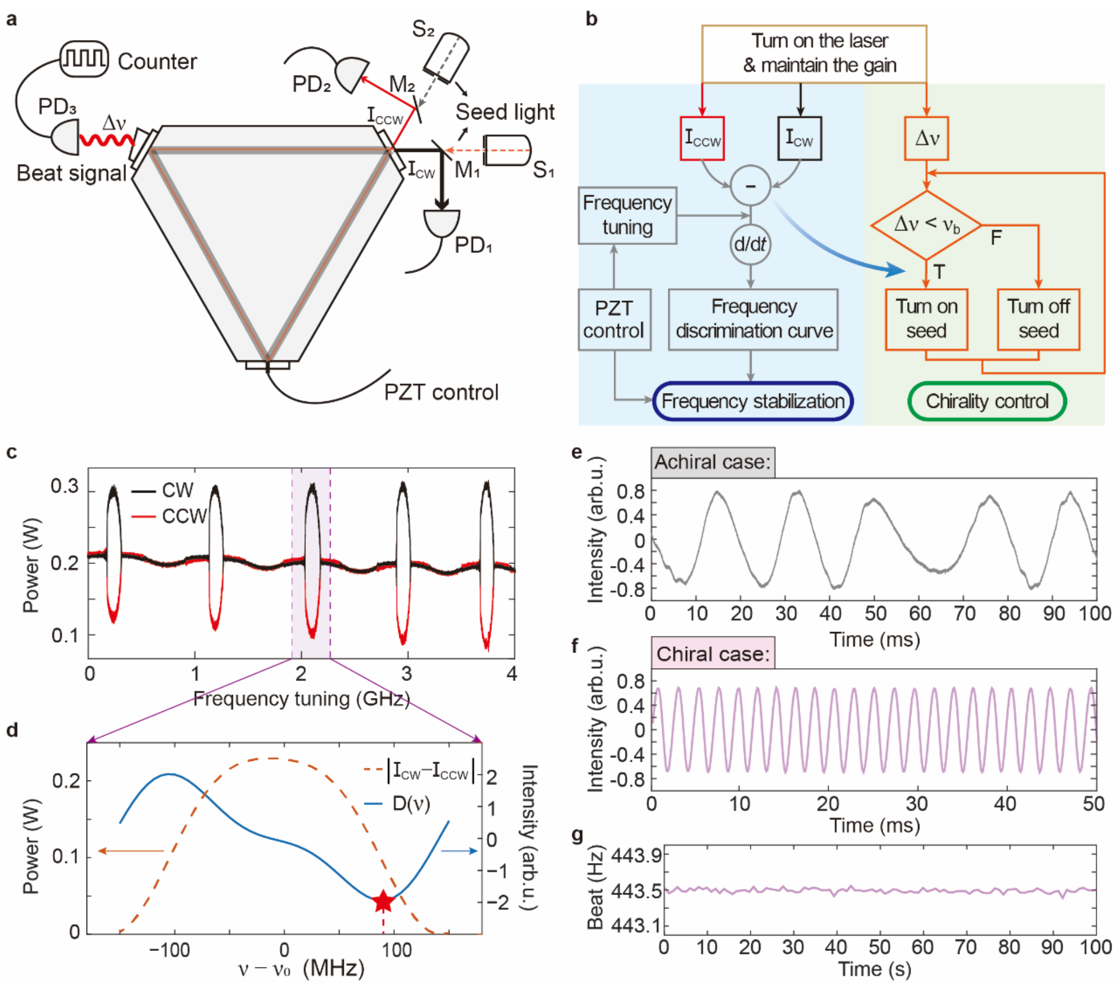

Fig. S5| Raw output signals and control strategies of the chiral RLG. a, Schematic of the signal readout and chirality control for the chiral RLG. PD1, PD2, and PD3 are photodetectors, measuring the CW laser intensity (I_{CW}), CCW laser intensity (I_{CCW}), and the beat signal $\Delta\nu$, respectively. The beat signal is then shaped and fed into a frequency counter. M_1 and M_2 are beam splitters. S_1 and S_2 are the seed sources. PZT: piezoelectric transducer. **b**, Flowchart of the frequency stabilization and chiral control protocol. **c**, Full-range frequency tuning curves of laser intensity. Black and red curves represent the output power in the CW and CCW directions, respectively. The periodic pattern of chiral SSB indicates traversal of multiple longitudinal mode spacings during the unidirectional sweep of the PZT. **d**, Evolution of the intensity difference (orange curve) and the corresponding discrimination signal D(ν) (blue curve) as a function of laser frequency. The red star denotes the minimum of D(ν). **e**, Beat signal at a rotation rate of 0.04 °/s when the RLG is in the achiral state. **f**, Beat signal at the same rotation rate (0.04 °/s) when the RLG is in the chiral state. **g**, Continuous beat frequency over 100 seconds when the RLG is operated at the chiral state and stabilized at the point marked by the red star in panel **d**.

Below, we provide a detailed clarification of our experimental procedure.

1. **Identification of the operating point:**

As correctly noted by the reviewer, the initial chiral state of the RLG is inherently random upon startup. To address this, we first set the pump current to establish the desired gain level. We then carefully adjust the laser frequency to a specific operating point on the gain curve. According to our theoretical framework, chiral spontaneous symmetry breaking (SSB) occurs under the condition of $\alpha(\xi - 1) > 2r$. To precisely identify the operating point, we record the discriminator curve by plotting the differential value of the intensity difference between CW and CCW beams as a function of laser frequency (see Supplementary Fig. S5**d**). The extremum of this discriminator curve corresponds to the optimal operating point.

2. **Stabilization in the Desired Chiral State**:

As illustrated in Figs. S5**a** and **b**, we have provided a flowchart detailing the startup and frequency stabilization control methods for the chiral RLG. Initially, the He-Ne laser is turned on while maintaining a constant pump power, allowing simultaneous acquisition of the intensities of both CW and CCW beams and the beat signal $\Delta\nu$ via photodetectors PD1 to PD3. During the initialization process, the first step is to maintain the RLG's operating point on the right side of the gain curve. This is achieved by unidirectionally driving the piezoelectric transducer (PZT) to reduce the cavity length, thereby tuning the RLG toward higher frequency and achieving the mode-sweeping curve of the RLG (Fig. S5**c**). The system enters the right side of the gain curve when the difference between the CW and CCW intensities $|\mathrm{I_{CW}} - \mathrm{I_{CCW}}|$ passes through a maximum during frequency tuning.

Subsequently, as shown in Fig. S5**d**, a frequency discrimination curve D(ν) is derived by performing differentiation, amplification, and filtering on the sweeping curve of $|\mathrm{I_{CW}} - \mathrm{I_{CCW}}|$. Frequency stabilization of the RLG operating point is then achieved based on the minimum point in D(ν) (indicated by the red star in the figure).

Simultaneously, we continuously monitor the beat signal $\Delta\nu$ of the RLG. If beat signal $\Delta\nu$ is less than the frequency bias ν_b (indicating a chiral flip into the "thumbs-down" state), seed light is injected into the direction with the weaker laser intensity. This active intervention efficiently restored the system to the desired chiral state.

Revision: We fully agree with you that a detailed description of this procedure will enhance experimental reproducibility.

Accordingly, we have now added a comprehensive step-by-step protocol to the **Supplementary Information (Section S4)** to include specifics on operating point selection, frequency tuning, and seed light injection.

Thank you once again for this valuable suggestion, which has significantly improved the clarity of our methodological description.

Comment #5 A few points in Fig. 2:

5-a- I find the horizontal axes in Figs. 2c and 2e confusing. Specifically in Figure 2e, it is not clear whether 'Tuning Frequency' represents a new detuned lasing frequency or detuning from a reference point. To improve clarity and interpretability, I suggest that the authors replot these figures with explicit experimental values on their horizontal axes.

5-b- Additionally, it would be very helpful to add what the shaded regions mean in Fig. 2e. Are they standard deviations of measurements? It can be added to the caption.

5-c- In Fig. 2c what is the operating wavelength of the laser? It can be added to the caption.

5-d- In Fig. 2e what is the applied pump current? It can be added to the caption.

Responses #5:

The reviewer's comments on Fig. 2 have helped us improve the theoretical analysis, for which we are thankful. We address each point below:

Reply to 5-a:

We thank the reviewer for this important comment.

As suggested, we have replotted Figs. 2c and 2e with explicit experimental parameters indicated on the horizontal axes.

In Fig. 2e, the horizontal axis now clearly represents the frequency detuning relative to the gain center of the Ne^{20} atoms. As shown in the revised figures, the nonlinear coupling coefficient reaches its maximum when the laser frequency is tuned to the Ne gain center.

Reply to 5-b:

We agree with the reviewer that clarifying the shaded regions is important. These regions represent the standard deviation of the measured values, reflecting the range of intensity fluctuations during the continuous frequency tuning process.

We have added a note to the figure caption to explicitly state these regions.

Reply to 5-c:

The laser operating point (i.e., the wavelength) in Fig. 2**c** is ν_0, corresponding to the gain center of the Ne^{20} atoms.

This information has now been included in the revised caption.

Reply to 5-d:

The applied pump current in Fig. 2**e** is 0.6 mA.

This value has been added to the figure caption.

Thank you once again for these valuable suggestions. All the modifications mentioned above have been incorporated into the revised manuscript.

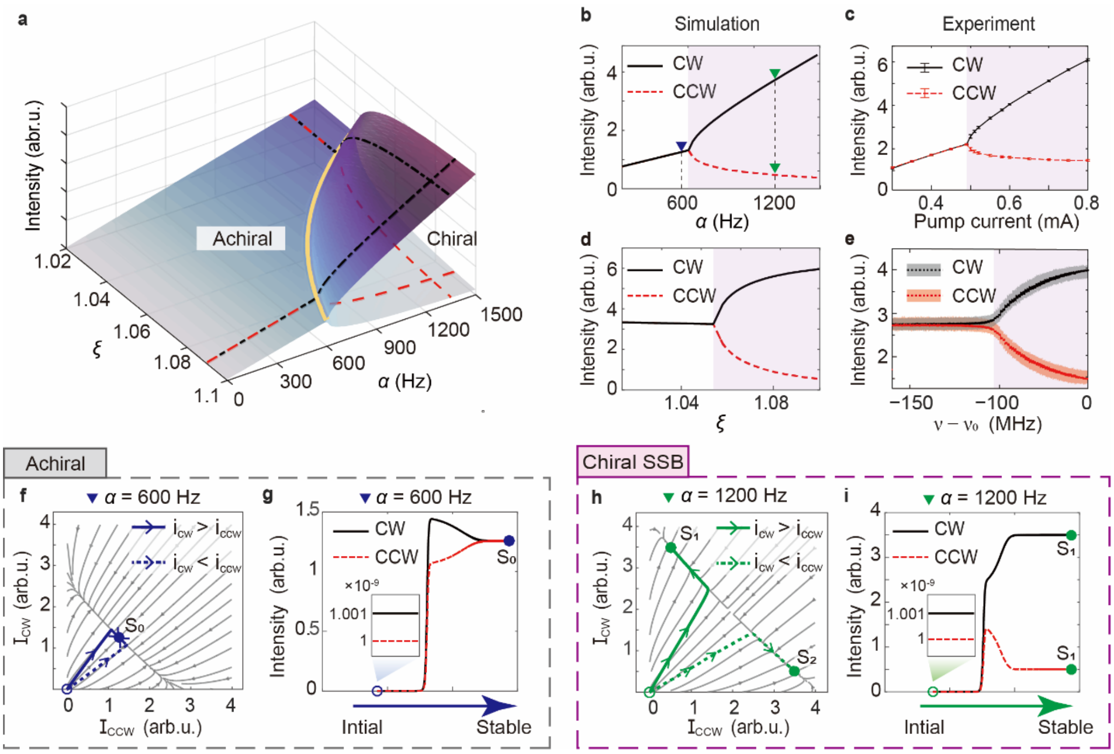

Fig. 2| Theoretical analysis of SSB in the ring laser. a, Phase diagram in two-parameter space (ξ: nonlinear coupling coefficient, α: net gain coefficient) demarcating symmetric (left of the yellow curve) and chiral SSB states (right). **b,** Simulated and **c,** experimental results of pitchfork bifurcation in CW/CCW intensities by increasing gain at ξ = 1.09 and $\nu = \nu_0$ respectively. ν_0 is the gain center frequency of the Ne^{20} atoms. **d,** Simulated and **e,** experimental results of pitchfork bifurcation by increasing the nonlinear coupling coefficient (or tuning frequency) at α = 1200 Hz and the pump current of 0.6 mA respectively. The shaded regions in **e** represent the fluctuation range of the laser light intensity (i.e., the standard deviation of the measurement results). **(f,g),** Symmetric state (α = 600 Hz): **f,** Phase diagram of the intensity evolution with one stable point (S_0), where i_{cw} and i_{ccw} are the minute initial intensity of CW and CCW mode respectively; **g,** Dynamic evolution of the CW and CCW mode intensities from the initial to the stable state. **(h,i),** Chiral SSB state (α = 1200 Hz): **h,** Phase diagram of the intensity evolution with two stable points (S_1 and S_2). **i,** Dynamic evolution of CW and CCW mode intensities from the initial to the stable state (S_1). In both **g** and **i,** i_{cw} exceeds i_{ccw} by 0.1%.

Comment #6 Detection Errors on Beat Response: Figure 4b, which presents critical beat note data, notably lacks any indication of measurement uncertainty (e.g., error bars). This contrasts with the inclusion of uncertainty for intensity data in other figures (e.g., Fig. 2c and Fig. 3b). Quantifying this uncertainty is crucial for a complete assessment of the RLG's high-precision performance, especially given two factors:

A- The method relies on precise sub-100 nm PZT mirror adjustment for bias point setting. Given the stated Zerodur coefficient of thermal expansion (CTE) of <5×10^{-6} /°C for the 150 mm cavity e.g., a 0.1°C temperature fluctuation could induce a cavity length change of ΔL = 75 nm = $0.15\text{m}\times5\times10^{-6}/°\text{C}\times0.1°\text{C}$. Such thermal drifts, along with other environmental factors or mechanical movements, could rapidly consume or exceed the available 100 nm adjustment range, directly impacting the frequency offset and introducing noise into the measured beat note.

B- The chiral biasing scheme inherently uses differential intensity (as detailed in Figures 2c and 3b), which may impact beat note signal contrast and thus the precision of its frequency determination.

Could the authors please clarify whether the beat note uncertainties in Figure 4b are really negligible, or alternatively, include error bars for the reported measurements?

Responses #6:

We thank the reviewer for raising these points regarding measurement uncertainties in our beat signal data and provide the following clarifications:

A. Thermal stability and cavity length control

We now specify the thermal expansion coefficient (CTE) of the Zerodur material used in our resonator cavity in the Methods section. In our experiments, we utilized ZERODUR® Expansion Class 0 (manufactured by SCHOTT AG, https://www.schott.com/en-us/products/zerodur-p1000269/technical-details), which has an ultra-low CTE of **2×10^{-8} /°C.**

For a cavity length of 0.375 m, a temperature fluctuation of 0.1°C results in a length change of **ΔL = 0.375 m × 2×10^{-8} /°C × 0.1°C = 0.75 nm**. This corresponds to a frequency drift of **less than 1 MHz**, which is negligible for the performance of our laser gyroscope. This exceptional thermal stability is one of the key reasons why ring laser gyroscopes possess high precision and reliability in industrial applications.

Regarding the PZT mirror adjustment range:

For the ring cavity length of 0.375m, a 100 nm tuning corresponds to approximately **126 MHz** of frequency tuning. Based on the mode-sweeping curve of the RLG in Fig. S5**c**, the actual available range of our piezoelectric transducer (PZT) is over **3.17 µm ≈ 4000 MHz / 126 MHz × 0.1 µm**, rather than the 100 nm range.

Revision: To avoid ambiguity, we have specified the full tuning range of the entire resonant cavity in the caption of Figure 1 (lines 54-59, page 3):

"The mirror associated with the piezoelectric transducer (PZT) enables nanometer-level cavity length tuning, with a total tuning range > 3 µm…a 100 nm displacement corresponds to about 126 MHz of frequency tuning in this cavity…"

B. Signal contrast and uncertainties of beat frequency in chiral states:

As shown in Fig. 4**a**, the maximum frequency bias does not occur at the point of maximum intensity asymmetry. Taking the operating point ν_3 in Fig.4**a** as an example, the output powers are **5 µW (CW)** and **3 µW (CCW)**, whose beat amplitude can be estimated as **3.873 µW**≈ $\sqrt{3^2+5^2}$ µW Compared to the beat amplitude of **4 µW** under achiral conditions, this represents only a **3.2% reduction in signal contrast**.

Furthermore, Fig. S5**f** (added to the Supplementary Materials, also given in our reply to your comment 4) displays the raw beat note signals measured with an AC detector at the operating point marked by red star in in Fig. S5**d**, demonstrating sufficient signal quality. In practice, commercial laser gyroscopes employ mature frequency counting techniques that convert the sinusoidal beat signal into a square wave for digital counting. Consequently, **variations in AC signal amplitude**

do not affect the frequency measurement precision. Figure S5g shows the frequency output from our counter. Under steady-state conditions, the standard deviation of the frequency measurement over 100 seconds was only 0.1 Hz (approximately 0.1% of the output signal), confirming that measurement uncertainties are negligible.

Given the exceptionally high stability of the beat frequency measurements and the minimal impact of amplitude variations on frequency counting, **the uncertainties in the data presented in Fig. 4b are indeed negligible**. Therefore, error bars are not essential for the interpretation of these results.

Revision: We have revised the main text and Supplementary Materials to include all these aforementioned details. Now we believe that these clarifications fully address the reviewer's concerns.

Comment #7 Robustness of Nanometer-Scale Bias Control in Dynamic Environments: The proposed biasing method effectively eliminates the need for mechanical dithering, which is a significant advantage. However, this technique relies on precise nanometer-scale tuning of a PZT-controlled mirror to set and maintain the laser frequency bias. In practical applications, such as those involving varying operational environments, even minute mechanical noise, thermal fluctuations (leading to thermal expansion/contraction), or other environmental perturbations could induce unintentional cavity length variations of this scale or larger. For example, a thermal drift in the studied RLG can be as high as ~750 nm/°C, based on the Zerodur CTE provided in Methods. While the stationary Allan plot analysis in Fig. 4d demonstrates excellent stability, possibly in a controlled and static environment, it does not fully capture performance under dynamic or perturbed conditions. It would be highly beneficial to explicitly address the potential impact of these external factors on the stability and performance of the chiral RLG, and comment on strategies for mitigating such effects if any.

Responses #7:

We thank the reviewer for raising this point regarding the robustness of our nanometer-scale bias control method in dynamic environments. We appreciate the opportunity to clarify the mechanisms that ensure the stability of our chiral laser gyroscope (RLG) under potential perturbations. Below, we address the concerns point by point:

1. **Common-mode noise suppression through single-longitudinal-mode operation**:

   Our chiral RLG operates in a single-longitudinal-mode state, meaning both CW and CCW beams propagate within the same longitudinal mode. This design inherently provides common-mode noise suppression. Environmental disturbances—such as mechanical vibrations or minor temperature fluctuations—affect both the CW and CCW beams similarly. Since the beat frequency signal is derived from the difference between these two beams, common-mode noise is effectively suppressed. This is a fundamental reason behind the ultra-high stability of laser gyroscopes. Importantly, the introduction of chirality (i.e., the intensity asymmetry between CW and CCW beams) does not compromise this common-mode suppression capability.

2. **Active stabilization systems for gain and operating point**:

We fully acknowledge that maintaining the chiral state (i.e., the intensity asymmetry) is crucial for stable frequency bias. To mitigate the effects of external perturbations (e.g., thermal drift or mechanical noise), we have concurrently considered maintaining the stability of both laser gain and frequency. Specifically, we continuously monitor the sum of the CW and CCW beam intensities and use this signal in a feedback loop to control the pump current, thereby stabilizing the gain. The operating point is stabilized by locking the laser frequency to the extremum of the discriminator curve (see Fig. S5 which is added to the Supplementary Materials, also given in our responses to your comment 4). Stabilizing to this extremum ensures robustness against minor cavity length changes.

a) **Robustness of the frequency bias against drift**:
As shown in Fig. 4a, the frequency bias curve is relatively flat around its maximum. Our analysis indicates that a frequency drift of **1 MHz** (e.g., due to cavity length change of **~1 nm**) results in a bias shift of only **~2.8 Hz**, which is less than **1%** of the total bias value. Given that our piezoelectric transducer (PZT) provides **nanometer-scale precision**, active frequency stabilization can readily compensate for such perturbations.

b) **Experimental Characterization of Gain Variation Impact**:
We experimentally investigated the effect of gain variations on frequency bias stability (Supplementary Fig. S6). At the operating point indicated by red star in Fig. S5**d** (i.e., the extreme point of frequency discrimination curve), a **5% change in gain** leads to a bias shift of **~10 Hz**, representing less than **4.2%** of the total bias value. This demonstrates that the system is reasonably tolerant to gain fluctuations.

In summary, the combination of **common-mode noise suppression** and our **active gain/frequency stabilization systems** ensures robust long-term operation of the chiral RLG in our experiment. We agree with the reviewer that dynamic environmental conditions warrant careful attention, more engineering optimizations and frequency stabilization strategies need to be designed specifically in the future to mitigate such effects.

Revision: We have added a discussion on these points to the Supplementary Materials **(Section S5)** to provide a more comprehensive assessment of robustness.

S5: Analysis of bias stability in the chiral RLG

The stability of this bias directly determines the gyroscope's bias instability. As calculated by the Allan deviation in Fig. 4d of the main text, the gyroscope's bias instability at 10 seconds under stationary conditions is 2.2×10^{-2} °/h, satisfying typical industrial application requirements.

Differing from the traditional achiral RLG, the frequency bias in the chiral RLG arises from spontaneous symmetry breaking. Given the unique nature of this biasing mechanism, we analyze the stability of the chiral RLG's frequency bias concerning two key factors influencing chiral SSB: laser frequency and gain.

Figure 4a in the main text shows the relationship between the frequency bias and laser frequency. Near the point of maximum bias, the change in bias induced by a shift in the operating point is relatively small: a frequency drift of 1 MHz corresponds to a bias change of approximately 2.8 Hz, which is less than 1% of the total bias. For the resonator with a perimeter of 375 mm in our work, a cavity length change of 1 nm corresponds to a bias shift of about 3 Hz. This level of control is readily achievable with PZTs offering nanometer-scale precision.

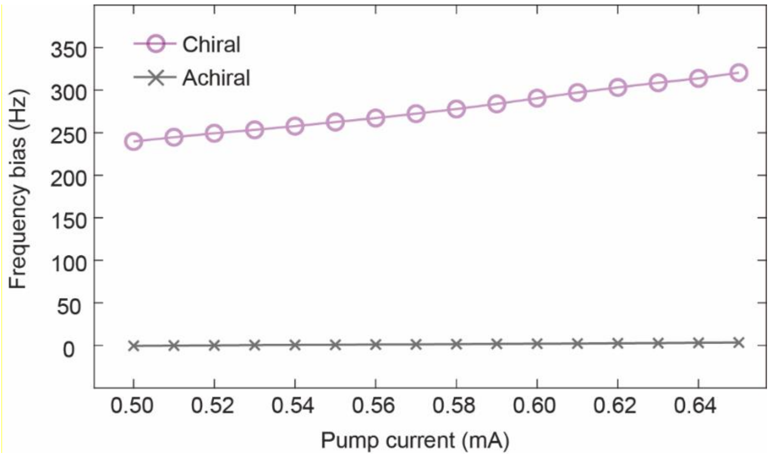

Fig. S6| Frequency drift of chiral and achiral RLGs under different pump currents

Figure S6 illustrates the impact of gain variation on the frequency bias. With the gyroscope stabilized at a certain operating point (i.e., the red star shown in Fig. S5**d**), the pink curve in Fig. S6 shows that increasing the current from 0.5 mA to 0.6 mA raises the frequency bias by about 50 Hz, correlating with an increased intensity asymmetry. Considering that current fluctuations from a stabilized power supply can be better than 1%, the corresponding fluctuation in the frequency bias is estimated to be around 2.5 Hz. In contrast, the beat frequency of the RLG in the achiral state is not affected by gain fluctuations.

In summary, for the chiral RLG presented in our work, typical frequency and gain drifts result in a variation of less than 1% in the frequency bias. Consequently, the chiral laser gyroscope imposes more stringent engineering requirements on gain stability and frequency stabilization methods compared to traditional laser gyroscopes.

Final Response:

Once again, we thank Reviewer #1 for the time and constructive comments, which have helped us to improve the clarity and completeness of our manuscript.

Responses to the comments of Referee #2&#3

Referees #2&#3:

Anamnesis:

The manuscript's main result is the experimental proof that a ring-laser-gyroscope (RLG) can operate at very low rotational speed, lasing on a single He-Ne^{20} isotope. Usually, these devices in this configuration cannot measure low rotational speed due to the mode lock-in phenomenon that prevents setting a frequency difference among the two counter-propagating modes in an active Sagnac interferometer. The experimental proof is complemented by a detailed theoretical analysis of the system and some numerical simulations.

The abstract introduces the self-locking problem affecting RLGs at low rotation rates and the reported solution. The main text then starts with a nod to RLG's history, then focuses on the locking issue and the approaches adopted so far to overcome it. Before entering the core of their work, the authors recap chiral systems in optics and their potential applications.

The manuscript core is essentially divided into two parts. The first concerns the asymmetric behaviour (chirality) of the ring laser cavity, the second discusses its impact on the performance of the chiral single isotope RLG at low rotation rates.

Main comments:

The paper results are surely novel and scientifically sound. They may be of interest to a pretty large audience, spanning physicists, engineers and more generally navigation experts. The main claim, which, after reading the paper twice, became clear, is the possibility of employing an RLG at low rotation rates. However, some shortcomings deserve consideration:

Response:

We are deeply grateful to the reviewers for their thorough and positive assessment of our manuscript. We truly appreciate their recognition of the novelty, scientific soundness, and potential broad impact of our work on employing chiral laser gyroscopes to break the lock-in limit.

We also thank the reviewers for their constructive feedback regarding the clarity of our main claim. We acknowledge this point and have thoroughly revised the manuscript to ensure that the central message is presented with maximum clarity and prominence from the introduction onwards.

In the following pages, we provide a detailed, point-by-point response to each of the specific comments raised. We have performed additional analyses, clarified the text, and refined the figures as needed. We are confident that these revisions have addressed the reviewers' concerns and significantly strengthened the overall presentation of our work.

Comment #1 The most important, in our opinion, is the possibility of controlling the proportionality factor, also known as the scale factor, between the rotation rate and the Sagnac frequency in a replicable, reliable and sufficiently precise manner. This implies including in the manuscript a detailed description of the relation among cavity detuning, RLG working point (e.g. pump power and gas pressure) and the non-linear parameter ξ. The interplay between these experimental quantities is evident all over the paper, but an explicit, auto-consistent analysis is missed. This absence prevents the possibility of a complete evaluation of the replicability and the sensitivity of the system. We refer to: a) the connection (Fig.1f) between non-linear coupling and frequency separation and the ratio between the intensities of CW and CCW beams; b) the relation between α (net gain coefficient) and pump current (Fig.2c-d); c) the relation between ξ and tuning frequency (Fig. 2d-e). All these experimental figures play a role in fixing the frequency bias, which in Fig. 4a is reported as a function of the detuning from the centre of the laser frequency, so that a much more clearer analysis of the interplay is necessary both from the theoretical and experimental point of views to support the effectiveness of the proposed method in terms of replicability.

Moreover, the sensitivity of the instrument is never assessed with respect to a change in the working conditions. What will happen to it if the pump power has a 5% stability in 1 hour? What happens if the cavity resonance drifts for some reason?

Responses #1:

We thank you for raising these points regarding the control of the scale factor and the system's replicability and sensitivity. We wish to first clarify the focus of our work: the chiral RLG proposed in this manuscript shares an identical structure with conventional two-frequency laser gyroscopes, which benefit from well-established manufacturing processes and performance standards. Consequently, its scale factor stability and operational reliability are consistent with those of industrial-grade devices. The primary innovation lies in the novel method for frequency biasing. **All parameters mentioned by the reviewer ultimately influence the bias repeatability and bias stability of the gyroscope**.

Below, we provide a point-by-point response to the specific issues raised.

Reply to points a), b), and c):

a) The logical chain in Fig. 1**f** illustrates that under fixed gain conditions, enhanced nonlinear coupling (controlled via the overlap of hole-burning areas, as shown in Fig. 1**c**) induces chiral SSB, leading to an intensity imbalance between the CW and CCW beams and consequent frequency splitting. The relationship between intensity asymmetry and nonlinear coupling is given by Equation (4), while the frequency splitting exhibits a near-linear dependence on the intensity difference, characterized by the parameter η in Fig. 4**a** and discussed in detail in the Supplementary Material:

$$\eta = \rho - \tau = -g\frac{c\kappa}{2L}\left[\frac{dZ_{\mathrm{i}}(\varepsilon)}{d\varepsilon} + \frac{\varepsilon}{\kappa^2+\varepsilon^2}Z_{\mathrm{i}}(\varepsilon)\right]$$

where g is the gain factor, c is the speed of light, L is the length of the laser cavity, κ is the ratio of the homogeneous broadening to Doppler broadening, $Z_{\mathrm{i}}(\varepsilon)$ is defined as the imaginary parts of the plasma dispersion function $Z(\varepsilon)$, and ε is the frequency parameter.

To avoid the complexity of laser physics and solving nonlinear differential equations, we provide numerical simulations and qualitative descriptions of these relationships.

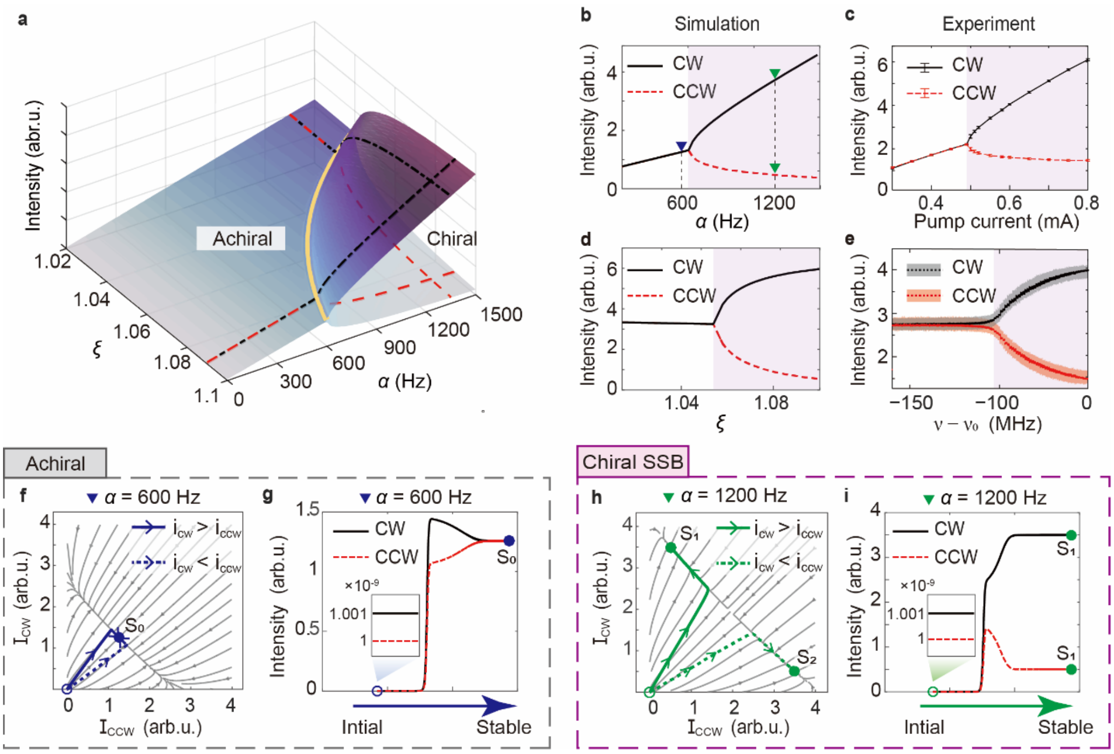

Fig. 2| Theoretical analysis of SSB in the ring laser. a, Phase diagram in two-parameter space (ξ: nonlinear coupling coefficient, α: net gain coefficient) demarcating symmetric (left of the yellow curve) and chiral SSB states (right). **b,** Simulated and **c,** experimental results of pitchfork bifurcation in CW/CCW intensities by increasing gain at ξ = 1.09 and $\nu = \nu_0$ respectively. ν_0 is the gain center frequency of the Ne^{20} atoms. **d,** Simulated and **e,** experimental results of pitchfork bifurcation by increasing the nonlinear coupling coefficient (or tuning frequency) at α = 1200 Hz and the pump current of 0.6 mA respectively. The shaded regions in **e** represent the fluctuation range of the laser light intensity (i.e., the standard deviation of the measurement results). **(f,g),** Symmetric state (α = 600 Hz): **f,** Phase diagram of the intensity evolution with one stable point (S_0), where i_{cw} and i_{ccw} are the minute initial intensity of CW and CCW mode respectively; **g,** Dynamic evolution of the CW and CCW mode intensities from the initial to the stable state. **(h,i),** Chiral SSB state (α = 1200 Hz): **h,** Phase diagram of the intensity evolution with two stable points (S_1 and S_2). **i,** Dynamic evolution of CW and CCW mode intensities from the initial to the stable state (S_1). In both **g** and **i**, $\mathrm{i_{cw}}$ exceeds $\mathrm{i_{ccw}}$ by 0.1%.

b) and c) We have replotted Fig. 2, adding explicit experimental data to the horizontal axes of Figs. 2**c** and 2**e** for direct comparison with theoretical calculations. The parameter α represents the net gain coefficient (i.e., the difference between gain and cavity loss), which is proportional to the pump current within the gain range (0.4~0.8 mA) studied in this work. The parameter ξ is defined as the ratio of self- to cross-saturation coefficients. Their relationship with the tuning frequency is discussed in the Supplementary Material. Further detailed theoretical foundations can be found in Chapters 9 to 11 of ***Laser Physics*** written by Sargent, Scully and Lamb.

Regarding sensitivity to changing working conditions:

We have further evaluated the effects of temperature variations, cavity drift, and gain fluctuations on the frequency bias in the main text and Supplementary Material.

- The cavity is fabricated using ZERODUR® Glass-Ceramic (Expansion Class 0) from Schott AG, which has an extremely low coefficient of thermal expansion (CTE ≈ 2×10^{-8} /°C). Thus, temperature fluctuations within room temperature ranges induce minimal cavity length changes (e.g., a 1°C change results in ΔL ≈ 7.5 nm for a 0.375 m perimeter cavity, corresponding to a frequency drift < 10 MHz).

  Revision: We have added the related discussion in the **Methods** part (lines 275-281, page 14):

  "**Fabrication of the He-Ne^{20} single-isotope RLG**

  The ring cavity of the laser gyroscope is fabricated from a single block of Zerodur glass (coefficient of thermal expansion ≤ 2×10^{-8} /°C, ZERODUR® Expansion Class 0 | SCHOTT), which provides remarkable dimensional stability under temperature variations. For a cavity length of 0.375 m, a temperature fluctuation of 0.1°C results in a length change of ΔL = 0.375 m × 2×10^{-8} /°C × 0.1°C = 0.75 nm. This corresponds to a frequency drift of less than 1 MHz.

  The optical cavity itself ensures a closed optical path through high machining precision, with the angular errors at its three corners controlled within 5 arcseconds and the length errors of its three sides maintained below 1 μm…"

- As shown in Fig. 4**a**, near the point of maximum frequency bias, the shift in operating point due to such drift causes a relatively small change in the frequency bias. The frequency interval between adjacent data points in the figure is 6.25 MHz (corresponding to a cavity length change of ~5 nm), while the induced bias drift is less than 10 Hz, accounting for less than 5% of the total bias. This level of drift can be effectively compensated by the piezoelectric transducer (PZT), which offers nanometer-scale control for frequency stabilization.

- We experimentally measured the impact of gain variation on the frequency bias. As shown in Fig. S7 of the Supplementary Material, under the chiral symmetry breaking condition, a 5% change in gain leads to a bias drift of approximately 35 Hz, which is less than 10% of the total frequency bias.

In summary, for the chiral RLG presented in this work, a reliable gain control and frequency stabilization system is the key factor determining its long-term stability.

Revision: We have incorporated these discussions and clarifications into the **Supplementary Materials Section 5** to enhance clarity regarding replicability and sensitivity.

S5: Analysis of bias stability in the chiral RLG

The stability of this bias directly determines the gyroscope's bias instability. As calculated by the Allan deviation in Fig. 4d of the main text, the gyroscope's bias instability at 10 seconds under stationary conditions is 2.2×10^{-2} °/h, satisfying typical industrial application requirements.

Differing from the traditional achiral RLG, the frequency bias in the chiral RLG arises from spontaneous symmetry breaking. Given the unique nature of this biasing mechanism, we analyze the stability of the chiral RLG's frequency bias concerning two key factors influencing chiral SSB: laser frequency and gain.

Figure 4a in the main text shows the relationship between the frequency bias and laser frequency. Near the point of maximum bias, the change in bias induced by a shift in the operating point is relatively small: a frequency drift of 1 MHz corresponds to a bias change of approximately 2.8 Hz, which is less than 1% of the total bias. For the resonator with a perimeter of 375 mm in our work, a cavity length change of 1 nm corresponds to a bias shift of about 3 Hz. This level of control is readily achievable with PZTs offering nanometer-scale precision.

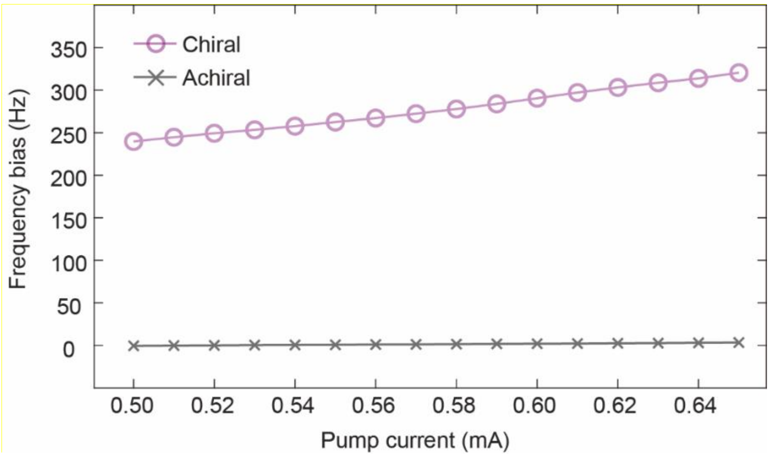

Fig. S6| Frequency drift of chiral and achiral RLGs under different pump currents

Figure S6 illustrates the impact of gain variation on the frequency bias. With the gyroscope stabilized at a certain operating point (i.e., the red star shown in Fig. S5d), the pink curve in Fig. S6 shows that increasing the current from 0.5 mA to 0.6 mA raises the frequency bias by about 50 Hz, correlating with an increased intensity asymmetry. Considering that current fluctuations from a stabilized power supply can be better than 1%, the corresponding fluctuation in the frequency bias is estimated to be around 2.5 Hz. In contrast, the beat frequency of the RLG in the achiral state is not affected by gain fluctuations.

In summary, for the chiral RLG presented in our work, typical frequency and gain drifts result in a variation of less than 1% in the frequency bias. Consequently, the chiral laser gyroscope imposes more stringent engineering requirements on gain stability and frequency stabilization methods compared to traditional laser gyroscope.

Comment #2 The second shortcoming regards the SSB regime. From Eq. (3) is clear that a change in the sign of (Icw - Iccw) affects the measured frequency difference, thus making the instrument unreliable if this sign is assigned randomly at the switching on of the instrument. It is not clear, from the actual text, if the authors suggest circumventing this by systematically using the second analysed method, 'rotation-induced controllable chirality,' or if the two methods can be used interchangeably and other 'tricks' can be used. In the former case, if we got it right, the claim that the presented system does not require external components would fail, as it would include a rotation stage."

Responses #2:

We appreciate your comments regarding the SSB and the potential uncertainty in the sign of (I_{CW} – I_{CCW}) upon startup. We agree that ensuring deterministic chirality is crucial for reliable operation. Below, we provide a clarification of our approach.

In practice, a truly random chirality at startup occurs only when the gyroscope is in a completely stationary state. However, for inertial sensing units, such a perfectly static condition is rarely encountered. **In our experiments, we employ a specific strategy to systematically induce the desired chirality, as shown in the added Fig. S5 in the Supplementary Materials.**

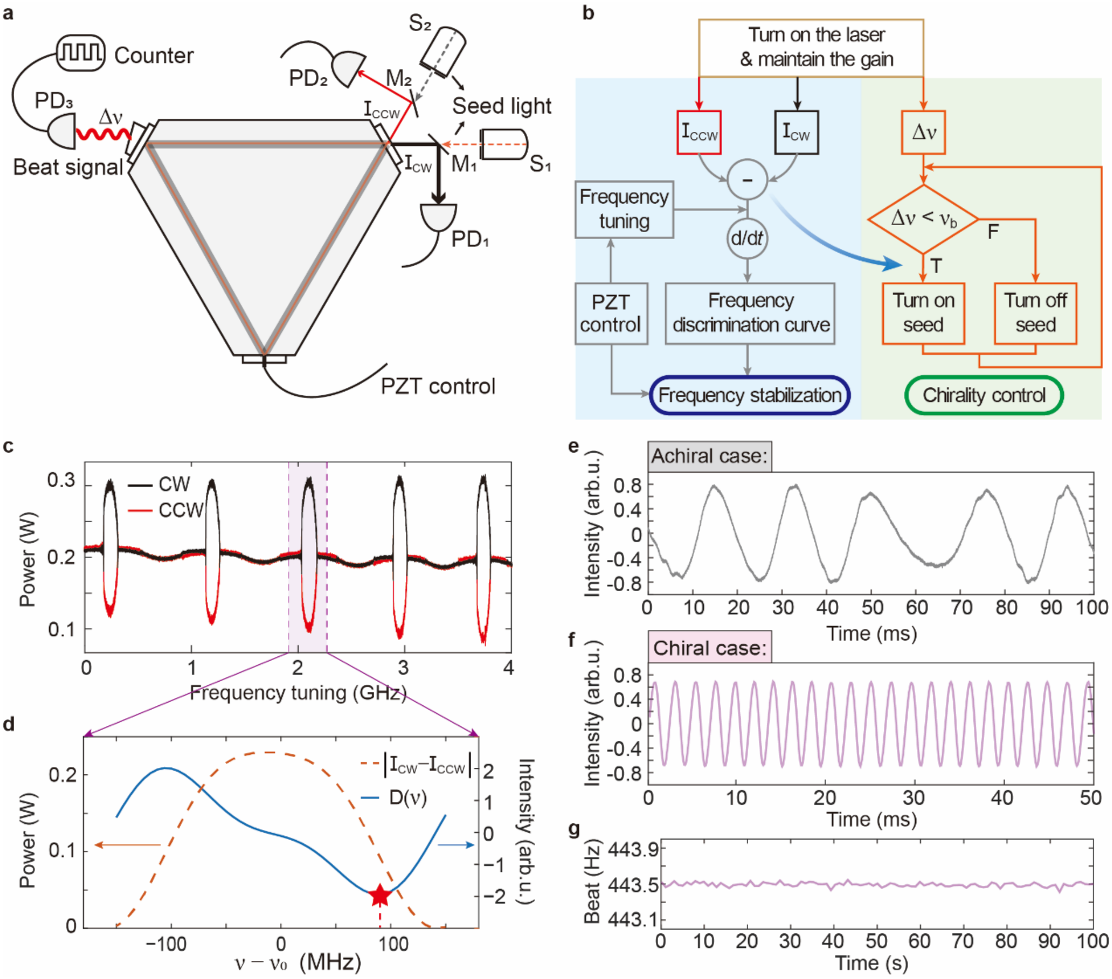

Fig. S5| Raw output signals and control strategies of the chiral RLG. a, Schematic of the signal readout and chirality control for the chiral RLG. PD1, PD2, and PD3 are photodetectors, measuring the CW laser intensity (I_{CW}), CCW laser intensity (I_{CCW}), and the beat signal $\Delta\nu$, respectively. The beat signal is then shaped and fed into a frequency counter. M_1 and M_2 are beam splitters. S_1 and S_2 are seed sources. PZT: piezoelectric transducer. **b**, Flowchart of the frequency stabilization and chiral control protocol. **c**, Full-range frequency tuning curves of laser intensity. Black and red curves represent the output power in the CW and CCW directions, respectively. The periodic pattern of chiral SSB indicates traversal of multiple longitudinal mode spacings during the unidirectional sweep of the PZT. **d**, Evolution of the intensity difference (orange curve) and the corresponding discrimination signal D(ν) (blue curve) as a function of laser frequency. The red star denotes the minimum of D(ν). **e**, Beat signal at a rotation rate of 0.04 °/s when the RLG is in the achiral state. **f**, Beat signal at the same rotation rate (0.04 °/s) when the RLG is in the chiral state. **g**, Continuous beat frequency over 100 seconds when the RLG is operated at the chiral state and stabilized at the point marked by the red star in panel **d**.

As depicted in Fig. S5**b**, the procedure is as follows: First, the laser is turned on with a constant pump power. Then, by monitoring the difference in intensity between the CW and CCW beams as the laser frequency is tuned, we actively control the gyroscope to operate on the **right side of the Ne gain center**. This is achieved by unidirectionally driving the piezoelectric transducer (PZT) to reduce the cavity length, thereby shifting the lasing frequency higher. The system is confirmed to be on the right side of the gain curve when the intensity difference ($I_{CW} – I_{CCW}$) passes through an extremum during frequency tuning.

When the gyroscope operates on the right side of the gain curve, the rotation-induced gain difference (as illustrated in Fig. 4**c** of the manuscript) biases the system towards a specific chiral state. Simultaneously, we continuously monitor the beat note signal. If the beat frequency drops below the bias value (indicating a chiral flip into the negative bias state), we inject seed light into the direction with weaker intensity. Theoretical calculations in Fig. 2**i** indicate that the final chiral state depends on the relative initial strengths of the laser modes, and seed light injection can effectively enhance these initial values, thereby actively restoring the desired chirality and ensuring operational stability.

It is worth noting that related technical aspects are under patent application. We also acknowledge the reviewer's point regarding future engineering optimizations, and we are actively exploring more streamlined and efficient methods for chirality control.

Revision:

This method of '**seed light injection for chirality recovery**' has been added in the **Supplementary Material Section 4**. We emphasize that this component serves as an external control element for chirality switch and is not used to generate the frequency bias. Therefore, it does not compromise the gyroscope's inherent stability or structural simplicity.

Comment #3. A third one regards the instrument SNR. The unbalancing of the two beams inherently reduces the fringe contrast of the Sagnac signal. This leads to a reduction in the SNR of the instrument and then its precision. A discussion on the accuracy of the instrument and, in particular, on the effect of the intensity unbalance on it is an important issue that is missing in the text."

Responses #3:

We thank you for raising this important point regarding the impact of intensity imbalance on the signal-to-noise ratio (SNR) and overall precision of the instrument.

In our experiments, the degree of chirality is actively controlled. As shown in Fig. 4**a**, the point of maximum frequency bias does not coincide with the point of maximum intensity asymmetry. At this operating point, the output powers for the CW and CCW beams are approximately 5 μW and 3 μW, respectively. The resulting beat note amplitude can be estimated as 3.873 μW$\approx \sqrt{3^2+5^2}$ μW. Compared to the beat amplitude of 4 μW under achiral conditions, the fringe contrast of the interference signal experiences only a modest reduction of approximately 3.2%.

Furthermore, Figs. S5**e** and **f** in the Supplementary Material display the raw beat note signals measured using an AC detector at the frequency-stabilized operating point (indicated by the red star in Fig. S5d), under a rotation rate of 0.04°/s (which is close to the lock-in threshold). These figures demonstrate that the beat signal under the chiral condition maintains an excellent SNR. In contrast, the beat signal under the achiral condition, being very close to the gyroscope's lock-in threshold, exhibits significant distortion, which would severely compromise the frequency stability of the gyroscope.

Actually, commercial laser gyroscopes employ mature frequency counting techniques that convert the sinusoidal beat signal into a square wave for digital counting. Consequently, **variations in AC signal amplitude do not affect the frequency measurement precision**. Fig. S5g shows the frequency output from our counter. Under steady-state conditions, the **standard deviation of the frequency measurement over 100 seconds was only 0.1 Hz** (approximately 0.1% of the output signal), confirming that measurement uncertainties are negligible.

Revision:

We have also added an analysis of bias stability in the chiral RLG in the **Supplementary Materials S5**. Please refer to the response to comment **1**.

Comment #4 In addition, to justify a non-vanishing steady-state value of (Icw-Iccw $ in Eq. (3) for the frequency shift, the authors study the evolution of the intensities towards their stationary values in the section 'Spontaneous chiral symmetry breaking.' The analysis is based on Eq. (1) in the main manuscript, or more precisely, Eq. (S1) in the Supplementary Material. In these equations, contrary to what happens in the cited references and in standard RLG models (e.g. the review of Wilkinson 1987 https://doi.org/10.1016/0079-6727(87)90003-6), the evolution of the intensities looks uncoupled from the phases. This approach, not explicitly mentioned in the text, requires a clear justification. Moreover, it is unclear how the connection between $ Icw-Iccw $ and the phase difference appears in Eq. (3) (see comment 2) if the two dynamics are completely uncoupled."

Responses #4:

We thank the reviewer for this insightful comment regarding the coupling between intensity and phase dynamics in our theoretical model. We acknowledge that the original manuscript did not provide a sufficiently complete treatment of this aspect.

In response to your valuable feedback, we have thoroughly re-derived the self-consistent equations and the corresponding linearized matrix relations. Particularly, we have revised our theoretical analysis with reference to established principles from [Wilkinson J R. Ring lasers. *Progress in Quantum Electronics*, 1987, 11(1): 1-103] and have cited this work accordingly. The revised derivation unifies the intensity and phase dynamics within a single framework and, importantly, **removes the prior assumption that the parameter *r* is a small quantity**.

Revision:

The updated results and the complete derivation process have been incorporated into both the Supplementary Material and the main text. We believe these revisions have significantly strengthened the theoretical foundation of our work.

S1: Solving the self-consistent equations of the ring lasers

In the main text, the third-order nonlinear equations for the counterpropagating complex electric fields $\tilde{E}_1$ and $\tilde{E}_2$ in a rotating ring laser with backscattering is written as Equation (1):

$$\begin{aligned}\frac{\partial}{\partial t}\tilde{E}_1 &= (\tilde{a} - \tilde{b}E_1^2 - \tilde{c}E_2^2)\tilde{E}_1 - i\Omega_S\tilde{E}_1 + r\tilde{E}_2 \\ \frac{\partial}{\partial t}\tilde{E}_2 &= (\tilde{a} - \tilde{b}E_2^2 - \tilde{c}E_1^2)\tilde{E}_2 + i\Omega_S\tilde{E}_2 + r\tilde{E}_1\end{aligned} \quad (1)$$

where $\tilde{E}_{1,2}(t) = E_{1,2}(t)\exp[-i(\omega t + \mu_{1,2}(t))]$, $\tilde{a} = \alpha + i\sigma$, $\tilde{b} = \beta + i\rho$, $\tilde{c} = \theta + i\tau$.

In this equation, $E_{1,2}$ and $\mu_{1,2}$ are the amplitudes and time-dependent phases of the CW and CCW lasing modes, respectively; ω is the resonant frequency of the ring cavity. The other parameters in the Equation (S1) are summarized in Table S1.

Table S1 Descriptions of Parameters in Equation (1) in the main text

Classifications	Parameters	Descriptions
Amplitude Parameters	r	Backscattering coupling coefficient
	α	Net gain coefficient
	β	Self-saturation coefficient
	θ	Cross-saturation coefficient
	$\boldsymbol{\xi = \theta/\beta}$	**Nonlinear coupling strength**
Frequency Parameters	Ω_S	Sagnac frequency shift
	σ	Frequency pulling coefficient
	ρ	Self-pushing coefficients
	τ	Cross-pushing coefficients
	$\boldsymbol{\eta = \rho - \tau}$	**Nonlinear frequency pulling**

By separating the real and imaginary parts of Equation (1), the dynamic equations for the amplitude and phase can be obtained, respectively:

$$\begin{aligned}\dot{E}_1 &= (\alpha - \beta E_1^2 - \theta E_2^2)E_1 + rE_2\cos\Delta u \\ \dot{E}_2 &= (\alpha - \beta E_2^2 - \theta E_1^2)E_2 + rE_1\cos\Delta u\end{aligned} \quad (S2)$$

$$\begin{aligned}\dot{\mu}_1 + \omega &= -\Omega_S + \sigma - \rho E_1^2 - \tau E_2^2 - r\frac{E_2}{E_1}\sin\Delta u \\ \dot{\mu}_2 + \omega &= \Omega_S + \sigma - \rho E_2^2 - \tau E_1^2 + r\frac{E_1}{E_2}\sin\Delta u\end{aligned} \quad (S3)$$

where $\Delta u = \mu_1 - \mu_1$, denoting the phase difference. The set of steady-state chiral solutions to the amplitude equations (S2) is given by：

$$E_1^2 \neq E_2^2, \quad E_1^2 + E_2^2 = \alpha/\beta \tag{S4}$$

A standard Adler equation can be obtained by subtracting the two equations in (S3):

$$\partial_t \Delta u = A - B\sin\Delta u \tag{S5}$$

Solving equation (S5), the expression for the phase difference Δu is obtained:

$$\tan(\Delta u/2) = \frac{1}{A}[B + \omega_B \tan(\omega_B t + \varphi_0)] \tag{S6}$$

where $\omega_B = \sqrt{A^2 - B^2}/2$ and φ_0 is an arbitrary constant. Let $I_{\mathrm{cw}} = E_1^2$, $I_{\mathrm{ccw}} = E_2^2$ and $\eta = \rho - \tau$. The coefficients A, B in equations (S5) and (S6) can be written as:

$$A = (\rho - \tau)(E_1^2 - E_2^2) + 2\Omega_S = \eta(I_{\mathrm{cw}} - I_{\mathrm{ccw}}) + 2\Omega_S$$
$$B = r\left(\frac{E_2}{E_1} + \frac{E_1}{E_2}\right) \tag{S7}$$

The beat frequency Δv is derived by taking the time average of the derivative of the phase difference[1]:

$$\Delta v = \langle \partial_t \Delta u \rangle = 2\omega_B = \sqrt{A^2 - B^2}$$
$$= \sqrt{[\eta(I_{\mathrm{cw}} - I_{\mathrm{ccw}}) + 2\Omega_S]^2 - \left(\frac{I_{\mathrm{cw}}}{I_{\mathrm{ccw}}} + \frac{I_{\mathrm{ccw}}}{I_{\mathrm{cw}}} + 2\right) r^2} \tag{S8}$$

For the achiral case (i.e., $I_{\mathrm{cw}} = I_{\mathrm{ccw}}$), the beat frequency calculated from the laser self-consistent equations[2–4] **exhibits exact agreement with** the result predicted by the linearized Hamiltonian matrix approach in equation (3) of the main text. For the chiral case, the discrepancy between the two methods is confined to the coefficient preceding r^2, which modifies the lock-in range. The frequency bias $\eta(I_{\mathrm{cw}} - I_{\mathrm{ccw}})$, however, is consistently given by for both approaches.

Textual comments

Comment #a. Line 22: The authors use "chiral spontaneous symmetry breaking" for the physical phenomenon underlying the whole manuscript, while at line 74, they use "spontaneous chiral symmetry breaking". We suggest using the same terminology throughout the paper.

Response #a:

Thank you for pointing out this discrepancy. We have unified the terminology to "**chiral spontaneous symmetry breaking**" throughout the entire manuscript.

Comment #b. Line 32: We suggest including more references on RLGs in Fundamental Physics experiments. A tentative, quite recent list can be extracted from https://doi.org/10.3389/frqst.2024.1363409.

Response #b:

Thank you for the suggestion. And we have added references on RLGs in fundamental physics experiments to the main text.

Revision:

"…has consistently played a pivotal role in ultra-high-precision inertial navigation systems, autonomous navigation platforms, and even fundamental scientific facilities[3–8]."

3. Di Virgilio, A. D. V. et al. Underground Sagnac gyroscope with sub-prad/s rotation rate sensitivity: Toward general relativity tests on Earth. Phys. Rev. Res. 2, 032069 (2020).

4. Capozziello, S. et al. Constraining theories of gravity by GINGER experiment. Eur. Phys. J. Plus 136, 394 (2021).

5. Benisty, D., Brax, P. & Davis, A.-C. Multiscale constraints on scalar-field couplings to matter: The geodetic and frame-dragging effects. Phys. Rev. D 108, 063031 (2023).

6. Igel, H. et al. ROMY: a multicomponent ring laser for geodesy and geophysics. Geophys. J. Int. 225, 684–698 (2021).

7. Schreiber, K. U., Kodet, J., Hugentobler, U., Klügel, T. & Wells, J. R. Variations in the Earth's rotation rate measured with a ring laser interferometer. Nat. Photonics 17, 1054–1058 (2023).

8. Giovinetti, F. et al. GINGERINO: a high sensitivity ring laser gyroscope for fundamental and quantum physics investigation. Front. Quantum Sci. Technol. 3, 1363409 (2024).

Comment #c Line 36: The references cited here (6-8) are not adequate in this context if the intent is to introduce the Sagnac effect to the general public, since none of those papers is a seminal work on the Sagnac effect. A general audience would benefit from a more pictorial explanation of the Sagnac effect and, possibly, citing some seminal and review papers (e.g. Wilkinson 1987 https://doi.org/10.1016/00796727(87)90003-6 is a review that starts with a historical part). References 6-8 should be moved elsewhere in the paper if appropriate.

Response #c:

We appreciate this suggestion. References 6-8 have been replaced by seminal and review papers related to Sagnac effect, as listed below:

"This beating signal originates from the Sagnac effect[7,8], which causes a frequency splitting between a pair of clockwise (CW) and counterclockwise (CCW) laser modes."

7. POST, E. J. Sagnac Effect. *Rev. Mod. Phys.* **39**, 475–493 (1967).

8. Wilkinson, J. R. Ring lasers. *Prog. Quantum Electron.* **11**, 1–103 (1987).

Comment #d Lines 41-43: Appropriate citations should be added for the two mentioned methods.

Response #d:

Thank you for this valuable suggestion. We have added appropriate citations for the two mentioned bias methods:

For the two-frequency mechanical dithered RLG:

Killpatrick, J. The laser gyro. IEEE Spectr.4, 44–55 (1967);

For the magneto-optically biased four-frequency differential RLG:

Statz, H., Dorschner, T. A., Holtz, M. & Smith, I. W. The Multioscillator Ring Laser Gyroscope. in Laser Handbook229–332 (Elsevier, 1985). doi:10.1016/B978-0-444-86927-2.50007-3.

Comment #e Line 45: We suggest moving the references to the end of the sentence.

Response #e:

The references have been moved to the end of the sentence as recommended.

Comment #f Lines 49-51, 69, 70: The concept of chiral for intensities, as far as we know, appears in Ref. 32, while in all the other cited papers, the term "chiral" is used in different contexts. We suggest stressing this point to avoid confusion in a non-specialised reader.

Response #f:

We thank the reviewer for this important comment. We have adjusted the text to clearly highlight the specific context of "chirality" used in our work concerning intensity symmetry breaking, distinguishing it from other uses in the cited literature. (lines 71-75, page 3-4)

"Among these diverse forms of asymmetry and chirality in nature and frontier research, as shown in Fig. 1**a**, our work focuses on breaking the intensity symmetry of counter-propagating modes in a ring laser gyroscope under single-longitudinal-mode operation via chiral spontaneously symmetry breaking (SSB)[31,32], thereby creating a fundamentally simpler, self-biased chiral laser gyroscope."

Comment #g Lines 84-85, eg. (1): Eq. (1) where field amplitudes appear as independent from the corresponding phases, contradicts the standard model for RLG (e.g. Ref. 38, cf. eq.. 2.3 and 2.4 in the dissipative case). Moreover, Eq. (1) can't be interpreted as a special case of Eq. (2.3) in Ref. 38 without assuming either a constant phase difference or r=0 (trivial case). If Eq. (1) is to be intended as an intentional deviation from the well-established models, we suggest motivating it and explicitly addressing it in the text. Eventually, we suggest specifying that the parameters in Eq. (1) are real constants.

Response #g:

We appreciate your comments regarding our theoretical derivation. We have thoroughly re-derived the self-consistent equations in the **Methods** section and **Supplementary Material S1**. Equation (1) is now a complex equation containing phase and intensity. Meanwhile, the parameters are also complex so that the complete behavior of the nonlinear coupled system could be described better.

Also, similar to the methodology in "Observation of the exceptional-point-enhanced Sagnac effect. *Nature* **576**, 65–69 (2019)", the linearized Hamiltonian [i.e., equation (2)] of a ring laser with non-zero dissipative backscattering can be derived from equation (1).

Moreover, our new derivation in **Supplementary Materials S1** demonstrates that the phase and amplitude equations can be separated into four equations, leading to a rigorous expression for the beat frequency without requiring approximation of the backscattering coefficient r.

Comment #h Lines 95-105 (caption of fig. 2): units are missing everywhere (even if the field amplitudes are dimensionless, the parameter α and r still have units of the inverse of the time). Why the value of r is never specified? Are the bifurcating surfaces and curves in Fig. 2.a,b,d showing the steady state intensity solutions of Eq. (1)? Are the simulations in Fig. 2.f too based on Eq. (1)? If yes, we suggest clarifying considering also the above comment (g.). Even if the experimental data shown in Figs. 2.e and 2.f qualitatively seem to follow the simulations in Figs. 2.b and 2.d, the scale chosen for the axis doesn't allow for appreciating whether the agreement is also quantitative.

Response #h:

We appreciate your comment regarding the missing units in Fig. 2 and your valuable suggestions.

Firstly, we provide the following clarification regarding the units. In our model, the field amplitudes are dimensionless, which is a common normalization in nonlinear optics models. We acknowledge that the parameters in the coupled mode equations, such as α and r, should have units of the inverse of the time (Hz). Based on the comparison with our experimental data (Fig. 4b), we determined that the backscattering coupling coefficient r is approximately 30 Hz. Consequently, all linear frequency parameters in our model required scaling. Specifically, the linear gain coefficient α, has also been scaled to maintain consistency with the physical system. On the other hand, the nonlinear coupling coefficient, $\xi = \theta/\beta$, represents the relative strength of cross- and self-saturation coefficients and is confirmed to be a dimensionless parameter.

Second, regarding the value of realistic backscattering ratio, in our actual laser gyroscope system with a total loss of approximately 68 ppm, the maximum estimated backscattering is less than 1 ppm, which is extremely small.

The theoretical plots in Fig. 2 are now based on Eq. (4) in the Methods section, which is derived from Eq. (1) using the separation of variables method for the amplitude equations.

The horizontal axes in Figs. 2**b** and 2**d** have been clearly quantified, and corresponding explanations have been added to the figure caption to facilitate quantitative comparison with the experimental data in Figs. 2**e** and 2**f**.

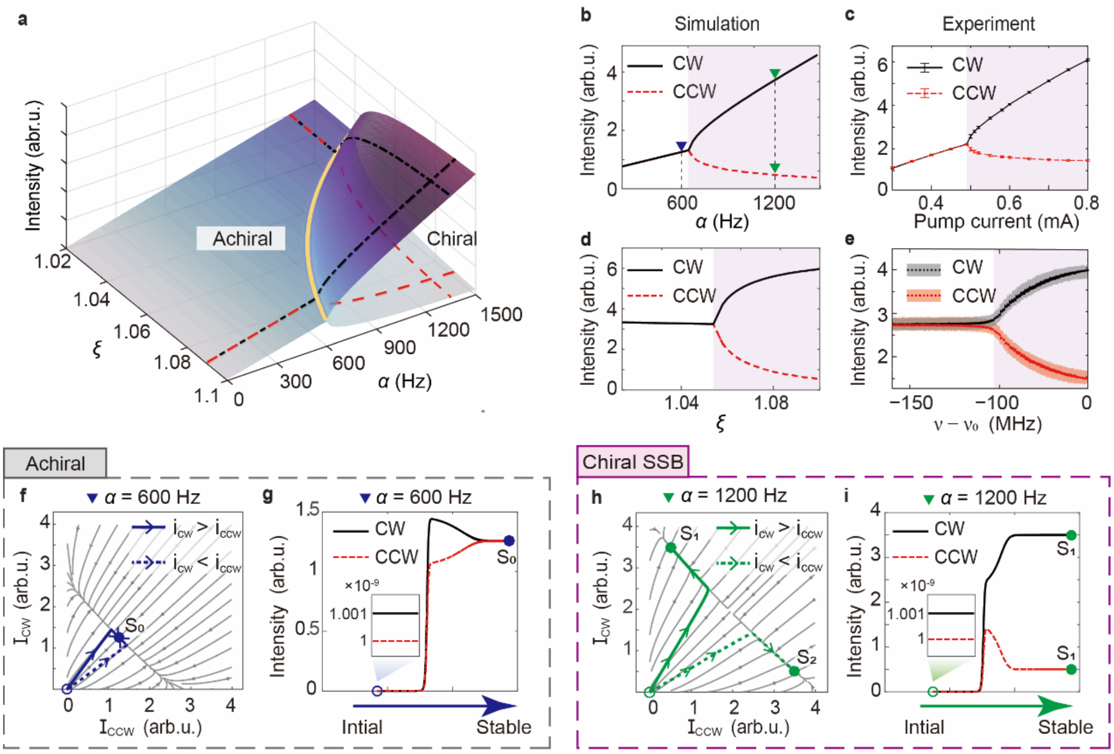

Fig. 2| Theoretical analysis of SSB in the ring laser. a, Phase diagram in two-parameter space (ξ: nonlinear coupling coefficient, α: net gain coefficient) demarcating symmetric (left of the yellow curve) and chiral SSB states (right). **b,** Simulated and **c,** experimental results of pitchfork bifurcation in CW/CCW intensities by increasing gain at $\xi = 1.09$ and $\nu = \nu_0$ respectively. ν_0 is the gain center frequency of the Ne^{20} atoms. **d,** Simulated and **e,** experimental results of pitchfork bifurcation by increasing the nonlinear coupling coefficient (or tuning frequency) at $\alpha = 1200$ Hz and the pump current of 0.6 mA respectively. The shaded regions in **e** represent the fluctuation range of the laser light intensity (i.e., the standard deviation of the measurement results). **(f,g),** Symmetric state (α = 600 Hz): **f,** Phase diagram of the intensity evolution with one stable point (S_0), where i_{cw} and i_{ccw} are the minute initial intensity of CW and CCW mode respectively; **g,** Dynamic evolution of the CW and CCW mode intensities from the initial to the stable state. **(h,i),** Chiral SSB state (α = 1200 Hz): **h,** Phase diagram of the intensity evolution with two stable points (S_1 and S_2). **i,** Dynamic evolution of CW and CCW mode intensities from the initial to the stable state (S_1). In both **g** and **i**, i_{cw} exceeds i_{ccw} by 0.1%.

In summary, we have updated all simulations with the correct, physically meaningful parameters. We wish to emphasize that this correction does not alter the fundamental physical phenomena or conclusions presented in our work. It primarily affects the absolute scaling on the frequency axes of the figures, bringing them into agreement with experimental values, while the relative behaviors and key results remain robust.

Comment #i Lines 114-119: It is not clear how α and ξ are related to the pump current and the tuning frequency, respectively (see main comment 1.).

Response #i:

The net gain coefficient α, defined as the difference between the total gain and total loss of the system, is proportional to the pump current within the gain range (0.4~0.8 mA) studied in this work. The parameter ξ is defined as the ratio of cross- to self-saturation coefficients. Their relationship with the tuning frequency is discussed in the Supplementary Material:

$$\xi = \theta/\beta$$

$$\theta = g\frac{\kappa^2}{\kappa^2+\varepsilon^2}Z_{\mathrm{i}}(\varepsilon)$$

$$\beta = g\left[Z_{\mathrm{i}}(\varepsilon) - \kappa\frac{dZ_{\mathrm{r}}(\varepsilon)}{d\varepsilon}\right]$$

where β and θ are self-and cross-saturation coefficients, which are related to the plasma dispersion function $Z(\varepsilon)$. ε is the normalized frequency parameter. Their relationship with the tuning frequency is discussed in the Supplementary Material S2.

Comment #j Lines 119-120: The evolutions in Fig. 2g and 2i are reported in time, but it is not clear if this is just the RLG running time since the switching on of the pump, or if, during that time, there is a tuning of some experimental parameters. Please clarify.

Response #j:

Thanks for raising this important point. These figures illustrate the dynamic process of the system evolving from an initial state to a steady-state solution based on the amplitude equations. The time coordinate does not represent the physical running time of the RLG but rather the convergence time of the numerical solution. To avoid misunderstanding, we have modified the labels on the horizontal axes in Figs.2**g** and 2**i**, accordingly.

Comment #k Lines 125.126: "Remarkably, as shown in Fig. 2i, a mere 0.1% initial intensity..." The scale adopted in Fig. 2i does not allow for seeing the initial imbalance. Either rephrase or add an inset to the figure.

Response #k:

We thank the reviewer for this suggestion. We have modified Fig. 2**i**, adding an inset to clearly show the initial intensity imbalance.

Comment #l Lines 136-142 (caption): colour scheme of Fig. 3e and 3f, and percentages in Fig. 3f are potentially misleading. We suggest using the same colours for the graphs and the arrows associated with the same rotation orientation. The matrix representation in Fig. 3f is not clear at first. We suggest specifying in the caption that in Figs. 3d and 3f, the modes with higher intensity are counted at each run.

Response #l:

Thank you for these valuable suggestions. We have adjusted the color scheme in Fig. 3. Throughout the figure, black now consistently represents the CW mode and red represents the CCW mode. Furthermore, we have added a clarification in the caption for Figs. 3d and 3f specifying that at each experimental run, only the mode with higher intensity was counted.

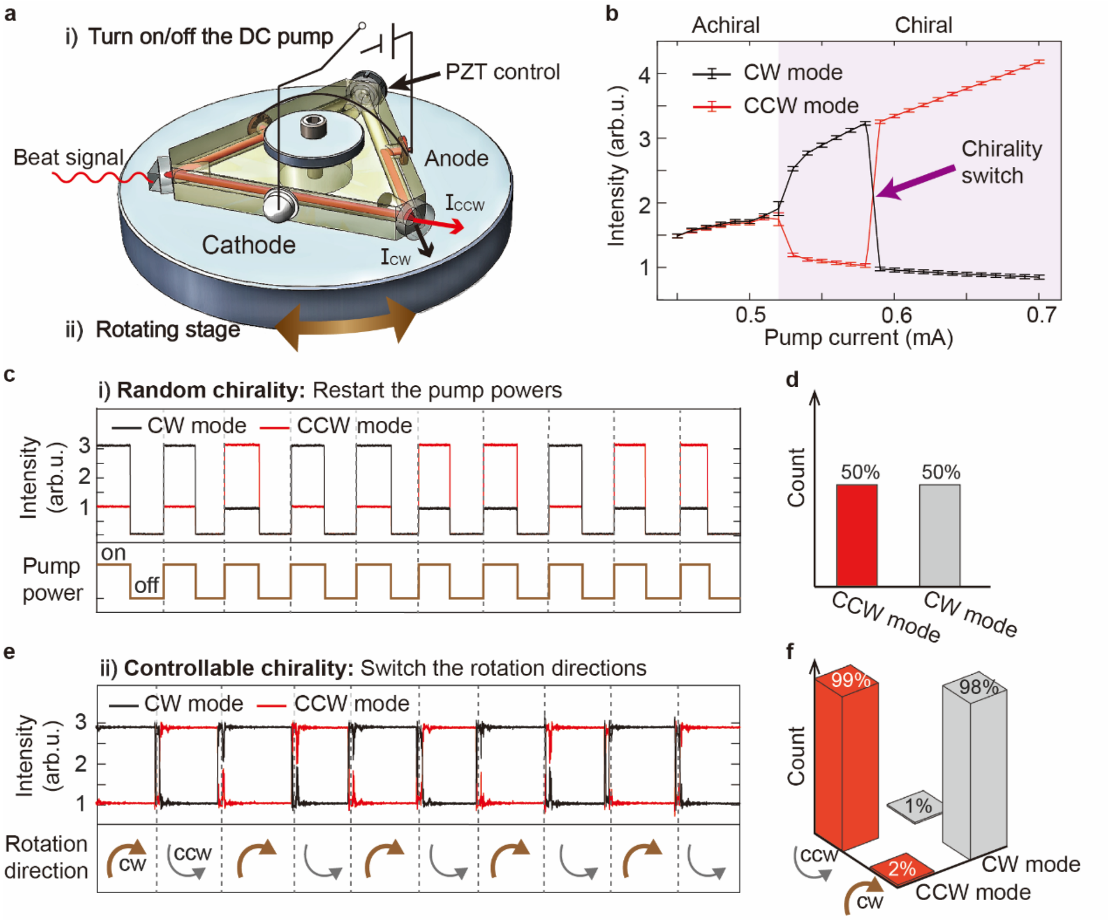

Fig. 3| Chirality switch in the chiral SSB phase of a He-Ne^{20} RLG. a, Experimental setup. Two methods: **i)** turning on/off the DC pump and **ii)** rotating the stage, are applied to induce a change in the chirality. **b,** Existence of bistable chirality in the chiral SSB phase under the stationary condition. **c,** Random chirality selections observed during periodic power cycling of the RLG and **d,** its corresponding statistical results. **e,** Regular and controllable chirality switches with uniform periodic oscillations of the RLG. and **f,** its corresponding statistical results. The statistical analyses for panels **d** and **f** are based on 200 experimental runs, and only the modes with higher intensity are counted in each run.

Comment #m Line 144-146: A "control paradigm" based on randomness is, in our view, a contradiction.

Response #m:

We agree with the reviewer's point. We have removed the phrase "control paradigm" and revised the relevant description in the text (lines 155-174, page 8):

"…This phenomenon serves as direct evidence for the existence of bistability in the chiral system. The following analysis will elucidate the switching dynamics of this bistable state under both stationary and rotating conditions…"

Comment #n Lines 155-156: The authors experimentally proved that in the SSB phase, there is a correlation between the direction of rotation of the RLG and the orientation of the mode with the highest stationary intensity. However, if field intensities are decoupled from the rotation in the theoretical model (cf. Eq. (1)), it is not clear how this can happen (see main comments 2. and 4.).

Response #n:

We thank the reviewer for this insightful comment. After separating variables for the real and imaginary parts of the self-consistent equations, the amplitude equations contain the phase term $\cos\Delta u$, rather than a rotation term Ω_S.

As shown in Fig. 4**c** of the main text, beyond the differential equations, the observed correlation between the gyroscope's chirality and rotation direction in our work can be attributed to the gain profile of the Ne^{20} atoms. When the laser operates on the right side of the gain curve, the frequency splitting due to the Sagnac effect causes the CW and CCW modes to experience different gains and initial values, leading to the observed rotation-dependent chiral characteristics according to the simulation results in Figs. 2**h** and 2**i.**

Comment #o Line 162: For the sake of clarity, a text comment, possibly with cross references, should address how Eqs. (2) and (3) are related to Eq. (1) and Eq. (S1) in the Supplementary Material. It is not clear how Δv is related to the phase difference and to Eq. (S2) in the Supplementary Material.

Response #o:

Thank you for your valuable comments. As mentioned before, we have significantly revised the theoretical section. Eqs. (2) and (3) are now derived from a linearized approximation of Eq. (1).

Furthermore, the beat frequency Δv is derived by taking the time average of the derivative of the phase difference Δu (referencing "Dynamics of a ring-laser gyroscope with backscattering. *Phys. Rev. A* **46**, 525–536 (1992)".):

$$\Delta v = \langle \partial_t \Delta u \rangle = \frac{1}{T}\int_0^T \frac{\partial \Delta u}{\partial t} dt$$

Comment #p Lines 193-197: Please improve the discussion of on Fig. 4b to help the reader in a full understanding of the different experimental curves, especially because the curves appear as connected and having the same colour in the plots.

Response #p:

Thank you for your kind reminder. We have improved the discussion of Fig. 4**b**:

"As depicted in Fig. 4**b**, the measured frequency responses show excellent linearity from −0.5 deg/s to 0.5 deg/s, differing only in the frequency bias values. In contrast, when the operating point is tuned to $\nu = \nu_a$ as shown in Fig. 4**a**, the gyroscope operating in the achiral state exhibits a nonlinear frequency response at rotation speed below 0.05 deg/s and enters the lock-in region when $\Omega < 0.03$ deg/s. Notably, a chirality flip occurs concurrently with the reversal of the rotation direction, which is consistent with the experimental results presented in Fig. 3**e**. Furthermore, to comprehensively validate the effect of chirality on the frequency bias, the chirality is artificially switched (such as restarting the power supply with a directional seed light) during clockwise rotation. As indicated by the "thumbs-down" region in Fig. 4**b**, this chirality-switched state produces a significant negative frequency bias, which in turn substantially increases the lock-in threshold of the RLG. The dashed curves in Fig. 4**b** show theoretical predictions from equation (3), demonstrating excellent agreement with experimental measurements."

Comment #q Lines 241-242: "...promising transformative impacts across metrology, integrated photonics, and quantum precision measurement systems". This sentence is too generic if not supported by references.

Response #q:

Thank you for your kind reminder. We have added relevant references to support the broader impact statement:

"In summary, this work bridges fundamental research in symmetry breaking with next-generation inertial sensing technologies, promising transformative impacts across metrology[46], integrated photonics[47,48], and quantum precision sensing systems[49,50]."

46. Frérot, I. & Roscilde, T. Symmetry: A Fundamental Resource for Quantum Coherence and Metrology. *Phys. Rev. Lett.* **133**, 260402 (2024).

47. Xu, G. *et al.* Spontaneous symmetry breaking of dissipative optical solitons in a two-component Kerr resonator. *Nat. Commun.* **12**, 1–9 (2021).

48. Lee, H. *et al.* Chiral exceptional point enhanced active tuning and nonreciprocity in micro-resonators. *Light Sci. Appl.* **14**, 45 (2025).

49. Kuffer, M., Zwick, A. & Álvarez, G. A. Sensing Out-of-Equilibrium and Quantum Non-Gaussian Environments via Induced Time-Reversal Symmetry Breaking on the Quantum-Probe Dynamics. *PRX Quantum* **6**, 020320 (2025).

50. Gao, H. *et al.* Signal amplification in a solid-state sensor through asymmetric many-body echo. *Nature* **646**, 68–73 (2025).

Comment #r Eq. (S1) in the Supplementary Material: General comment 4. applies. Moreover, the phases are real functions of time, so the last two equations in Eq. (S1) are inconsistent for values of r different from zero.

Comment #s Text before Eq. (S2) in the Supplementary Material: please give an estimation for the back-scattering ratio r to justify the assumption of a small quantity.

Response #r and #s:

We thank the reviewer for their careful attention to the theoretical derivation and for identifying the issues in our original version. As mentioned before, we have rederived the theoretical model presented in the revised **Methods and Supplementary Materials**. In the revised derivation, it is no longer necessary to approximate or ignore the backscattering coefficient *r*. As a result, the previously noted inconsistencies for non-zero values of *r* have been resolved.

Meanwhile, based on the comparison with our experimental data (Fig. 4b), we determined that the backscattering coupling coefficient *r* is approximately 30 Hz. The value of realistic backscattering ratio, in our actual laser gyroscope system with a total loss of approximately 68 ppm, the maximum estimated backscattering is less than 1 ppm, which is extremely small. Please also refer to the above Response #h.

Comment #t Eqs. (S3)-(S7) are obtained from Ref. 4-6. It would be of help to reference also where (page/section/Eqs) in the cited papers this model is given.

Response #t:

Thank you for this suggestion. While the calculation of the plasma dispersion function and nonlinear parameters in He–Ne lasers may vary in certain details across references, for a complete and detailed derivation, readers are referred to **Pages 150~159 and 176~179 in Chapters 9 to 11 of *Laser Physics* (1978)** written by Sargent, Scully and Lamb. We have added this comment in the Supplementary Material for clarity.

Eventual Comment The data complementing the manuscript are not of immediate use. Data for Fig. 2: i) the legend is missing, data cannot be easily interpreted; ii) file coupling: no indications on how the error bars are constructed, the legend is not clear; in particular, if the first column represents the pump current, why are its units "s"? iii) Data for Fig. 3b: why are the data on the x-axis in Fig. 3 b reported with units of mA, and in the table, they have units of s?

Response to Eventual Comment:

We thank the reviewer for pointing out the ambiguities in the original data descriptions, which has allowed us to clarify these important details. We apologize for any confusion caused by the incomplete legends. Below we provide a point-by-point response to the specific questions raised.

Clarification on the data files for Fig. 2 and Fig. 3b:

i) The data file named "c-increasing gain.csv" for Fig. 2c is organized as follows: The first column represents the pump current (in mA), the second and third columns contain the CCW optical intensity and its standard deviation, respectively, and the fourth and fifth columns contain the CW optical intensity and its standard deviation.

ii) Clarification on the "e-increasing coupling.CSV" dataset and error bars:

The data file named "e-increasing coupling.CSV" for Fig. 2**e** records the optical intensity variation under continuous linear frequency tuning. This data was acquired directly from an oscilloscope; therefore, the first column represents the **time (in seconds)** recorded by the oscilloscope, which corresponds to the frequency shift during the continuous tuning process.

The error bars were constructed from this continuous data stream. The data was grouped into segments of 100 consecutive points. The **average value** of each segment was used as the optical intensity measurement, and the **standard deviation** calculated from those 100 points was used as the error bar.

iii) The raw data for Fig. 3**b** was also acquired directly from the oscilloscope. As can be seen in the provided oscillogram, we measured the optical intensity continuously while ramping the pump current, which resulted in a series of small steps at equal time intervals. The data within each step corresponds to the optical intensity and its standard deviation measured at a specific pump current value in the main text figure. The pump current was controlled via external programming, which increased it linearly by 0.01 mA at fixed time intervals.

We have updated the data legends and the relevant descriptions to incorporate these clarifications.

Final Recommendation:

We believe that the actual manuscript can possibly be re-evaluated for publication in Nature, or in a more specific journal of the Nature group, after all the main shortcomings are completely

solved.

Final Response:

Once again, we extend our sincere gratitude to the reviewers #2 & #3 for their constructive feedback, which have been invaluable in helping us to strengthen the study and improve the clarity of our presentation. We believe that these results are very suitable for *Nature*.

Responses to the comments of Referee #4

Referee #4:

This paper proposes to solve the inherent lock-in effect in ring laser gyroscopes (RLGs) through spontaneous symmetry breaking (SSB) without requiring mechanical dithering or magneto-optic biasing elements. ***This represents a major innovation in traditional RLG design paradigms. With solid theoretical foundations and sufficient experimental data, it constitutes an excellent gyroscope-related paper.***

Response

We are deeply grateful to the reviewer for the exceptionally positive and insightful assessment of our work. We are truly encouraged by your recognition that our approach **"represents a major innovation in traditional RLG design paradigms"** and that the manuscript constitutes **"an excellent gyroscope-related paper"** with solid theoretical foundations and sufficient experimental data.

We are happy that our core message has been effectively communicated and its significance appreciated. We thank the reviewer once again for your time and for highlighting the strength and impact of our study. Below we provide a point-by-point response to the specific points raised.

Comment #1 The physical meaning of the nonlinear coupling coefficient ξ needs clarification in the main text, as it currently only appears in the appendix.

Response #1:

We thank the reviewer for this suggestion. The nonlinear coupling coefficient ξ is numerically defined as the ratio of the cross-saturation coefficient to the self-saturation coefficient. Physically, it reflects the degree of overlap of the hole-burning regions between the CW and CCW laser modes. As shown in Fig. 1**c**, a larger overlap region in the gain medium leads to increased competition for gain particles between the two modes, which manifests as an enhancement of the nonlinear coupling.

Revision:

We have now included this clarification in the main text (lines 96-99, page 5):

"In particular, α is proportional to the pump current within the gain range (0.4~0.8 mA) studied in this work and the nonlinear coupling coefficient ξ reflects the degree of overlap of the hole-burning regions between the CW and CCW laser modes as shown in Fig. 1**c**."

Comment #2 The physical mechanism of the nonlinear frequency pulling term η(Icw-lccw) in Equation (3) requires supplemental explanation.

Response #2:

We appreciate your comment about the nonlinear frequency pulling effect. As suggested, we have re-derived the linearized matrix from the equation (1) in the main text following the methodology referenced in [Lai et al., *Nature* **576**, 65–69 (2019)].

Revision:

The rederived main equations and ralative explanations (lines 84-91, page 4):

To elucidate the SSB mechanism in RLGs, we start from a third-order nonlinear dynamic equations for the dissipativly coupled counterpropagating waves[41–43]:

$$\frac{\partial}{\partial t}\tilde{E}_1 = \left(\tilde{a} - \tilde{b}E_1^2 - \tilde{c}E_2^2\right)\tilde{E}_1 + i\Omega_S\tilde{E}_1 + r\tilde{E}_2$$
$$\frac{\partial}{\partial t}\tilde{E}_2 = \left(\tilde{a} - \tilde{b}E_2^2 - \tilde{c}E_1^2\right)\tilde{E}_2 - i\Omega_S\tilde{E}_2 + r\tilde{E}_1 \tag{1}$$

where $\tilde{E}_{1,2}(t) = E_{1,2}(t)\exp[-i(\omega t + \mu_{1,2}(t))]$ represent the complex electric fields of the CW and CCW waves, with time-dependent amplitude $E_{1,2}(t)$ and phase $\mu_{1,2}(t)$; ω is resonant frequency of the ring cavity; Ω_S denotes the frequency shift caused by the Sagnac effect and r is the backscattering coupling coefficient. The real and imaginary parts of the complex parameters ($\tilde{a} = \alpha + i\sigma, \tilde{b} = \beta + i\rho, \tilde{c} = \theta + i\tau$), detailed in Table S1 of Supplementary Materials, represent the linear and nonlinear effects on the amplitude and phase, respectively.

The rederived approximate Hamitonian and explanations (lines 176-184, page 9):

Compared with traditional two-frequency RLGs, the beat frequency of the chiral RLG is completely different. Under the approximate gain clamping condition[44], the linearized Hamiltonian of a ring laser with non-zero dissipative backscattering can be derived from equation (1):

$$\boldsymbol{H} = \begin{bmatrix} -\Omega_S - \sigma + \rho I_{\text{cw}} + \tau I_{\text{ccw}} & ir \\ ir & \Omega_S - \sigma + \rho I_{\text{ccw}} + \tau I_{\text{cw}} \end{bmatrix} \tag{2}$$

where σ, ρ and τ are the imaginary parts of the complex parameters $\tilde{a}, \tilde{b}$, and $\tilde{c}$ in equation (1); $I_{\text{cw}} = E_1^2$ and $I_{\text{ccw}} = E_2^2$ are the intensity of CW and CCW laser modes, respectively; Ω_S is the frequency shift caused by Sagnac effect. The frequency difference between CW and CCW modes can be obtained by solving the eigenvalues $\lambda_\pm$ of $\boldsymbol{H}$:

$$\Delta v = \lambda_+ - \lambda_- = \sqrt{[\eta(I_{\text{cw}} - I_{\text{ccw}}) + 2\Omega_S]^2 - 4r^2} \tag{3}$$

where Δv is the beat frequency of the chiral RLG. Notably, the nonlinear frequency pulling coefficient, $\eta = \rho - \tau$, represents the overall effect of the laser intensity on its own frequency.

In addition, from the perspective of laser physics, the term η(Icw-Iccw) results from the combined effect of the self- and cross-pushing coefficients. These coefficients are related to the properties of the gain medium and represent a physical manifestation of the plasma dispersion function.

__Comment #3__ The abstract mentions this method would significantly advance all-solid-state laser gyroscopes, but the implementation is based on He-Ne lasers. Are the theoretical derivations universally applicable? Similarly, can this theory be extended to fiber-optic gyros or silicon-based microresonator gyros? This point should be rigorously discussed to attract broad interests to the laser gyroscope community.

Response #3:

Thank you for raising this important point regarding the general applicability of our method. Our experimental validation was conducted using a He-Ne laser gyroscope with a well-established industrial base, allowing for rapid validation and iteration of new physical concepts.

Although the SSB-enabled frequency biasing mechanism is fundamentally derived from the dynamics of ring lasers, in principle, it is applicable to any nonlinear coupled-wave systems. For solid systems, like fiber-optic gyros or silicon-based microresonator gyros, these methods could be extended and readily realized by introducing nonlinear couplings via optical or electrical pumping. Our approach thus offers a new pathway for developing future miniaturized, on-chip optical gyroscopes.

Revision:

We have included a discussion on the potential applications in the main text (lines 265-273, page 13):

"…Notably, the frequency bias of the chiral laser gyroscope is sensitive to fluctuations in the operating point and gain. This consideration becomes particularly critical in the context of on-chip optical gyroscopes, where strong mode coupling in solid-state systems may induce thermal effects that promote frequency drift. Therefore, for integrated on-chip implementations, further engineering efforts on robust gain control and advanced frequency stabilization techniques is essential to enhance the stability and reproducibility of chiral laser gyroscopes.

In summary, this work bridges fundamental research in symmetry breaking with next-generation inertial sensing technologies, promising transformative impacts across metrology[46], integrated photonics[47,48], and quantum precision sensing systems[49,50]."

Comment #4 Supplement discussion on challenges for solid-state implementation in experiments and potential solutions.

Response #4:

Thanks for your forward-looking suggestion. As you rightly point out in the sixth question, unlike the gas laser gyroscope (please find the response below), thermal effects pose a significant challenge for solid-state, on-chip implementations. In active systems, heat can cause drift of the resonator's operating frequency, affecting the stability of the frequency bias. Therefore, for on-chip gyroscopes, effective temperature control and frequency stabilization are crucial for maintaining stability. Furthermore, since the frequency bias characteristics are closely tied to the properties of the gain medium, future work should also focus on the control of solid-state gain media, such as the type and concentration of doping elements.

We have added a discussion on these challenges and potential solutions in the main text (lines 265-270, page 13):

"Notably, the frequency bias of the chiral laser gyroscope is sensitive to fluctuations in the operating point and gain. This consideration becomes particularly critical in the context of on-chip optical gyroscopes, where strong mode coupling in solid-state systems may induce thermal effects that promote frequency drift. Therefore, for integrated on-chip implementations, further engineering efforts on robust gain control and advanced frequency stabilization techniques is essential to enhance the stability and reproducibility of chiral laser gyroscopes."

Comment #5 The main text repeatedly uses "deg/h" while Figure 4d uses "°/h". The manuscript should standardize angular unit notation.

Response #5:

We thank the reviewer for pointing out this inconsistency. We have standardized the angular unit notation to " deg/h" in Fig. 4**d**:

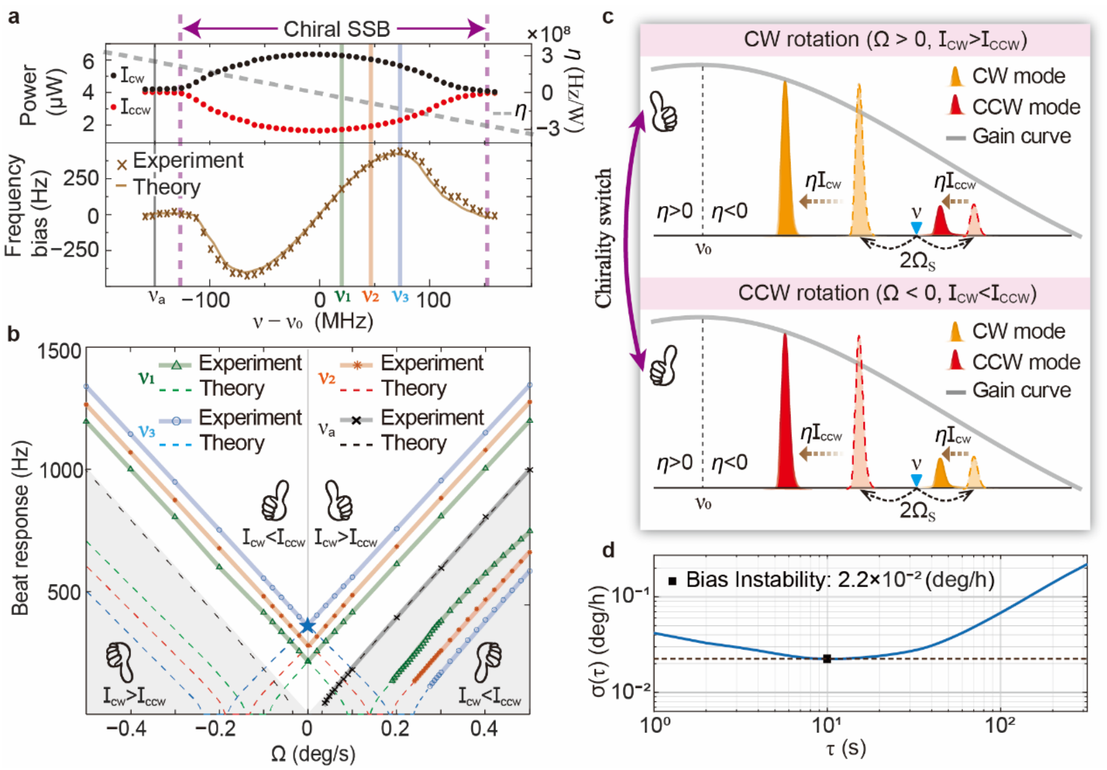

Fig. 4| Frequency response characteristics of the RLG in the chiral SSB phase. a, (upper panel) The CW/CCW mode intensity, nonlinear frequency pulling coefficients η and (lower panel) the corresponding frequency bias with tuning frequency ν around the Ne[20] gain center ν_0. **b,** The frequency response to low rotational speed of the RLG under different operating points and chirality states. ν_1, ν_2, ν_3 denote the chiral states and ν_a corresponds to the achiral state. **c,** Schematic of chirality switch and frequency bias principles for the RLG under CW/CCW rotation conditions. Ω_S is the frequency shift caused by Sagnac effect. **d,** Allan variance analysis of 1000-second frequency bias stability test at the operating point indicated by the blue star in **b**.

Comment #6 High-intensity mode competition may cause local thermal lensing effects, but the text doesn't discuss temperature drift impacts on cavity length stability. Was temperature control implemented during actual experiments?

Response #6:

We appreciate your insightful comments and questions. Unlike solid-state lasers, the thermal lensing effect is negligible in our gas laser using a low-pressure (6-8 Torr) He-Ne mixture as the gain medium. Moreover, the RLG cavity is fabricated from **ZERODUR® Glass-Ceramic (Expansion Class 0)** from Schott AG, which has an extremely low coefficient of thermal expansion (CTE ≈ 2×10^{-8} /°C). Consequently, temperature fluctuations within typical room temperature ranges induce minimal cavity length changes. For instance, a 1°C temperature change results in $\Delta L \approx 7.5$ nm for a cavity perimeter of 0.375 m, corresponding to a frequency drift of less than 10 MHz. Given these factors, active temperature control was not necessary in our experiments.

Revision:

We have added the above discussion in the Method (lines 277-281, page 14):

"The ring cavity of the laser gyroscope is fabricated from a single block of Zerodur glass (coefficient of thermal expansion ≤ 2×10^{-8} /°C, ZERODUR® Expansion Class 0 | SCHOTT), which provides remarkable dimensional stability under temperature variations. For a cavity length of 0.375 m, a temperature fluctuation of 0.1°C results in a length change of $\Delta L = 0.375\ \text{m} \times 2\times10^{-8}\ /°\text{C} \times 0.1°\text{C} = 0.75$ nm. This corresponds to a frequency drift of less than 1 MHz."

Comment #7 What is the stability limitation in Fig.4(d)? How can it be improved in the future?

Response #7:

Thanks for your perspective question. Since the chiral RLG operates without any external biasing components, it is inherently free from noise related to thermal drift or mechanical dithering. The primary factors limiting its long-term stability are the stability of the laser's operating point and the laser gain. Future improvements will focus on engineering optimizations of the frequency stabilization scheme for the chiral RLG to enhance its bias stability and practical applicability.

Revision:

Now we have added a description of the frequency stabilization method to the **Supplementary Material Section 4**.

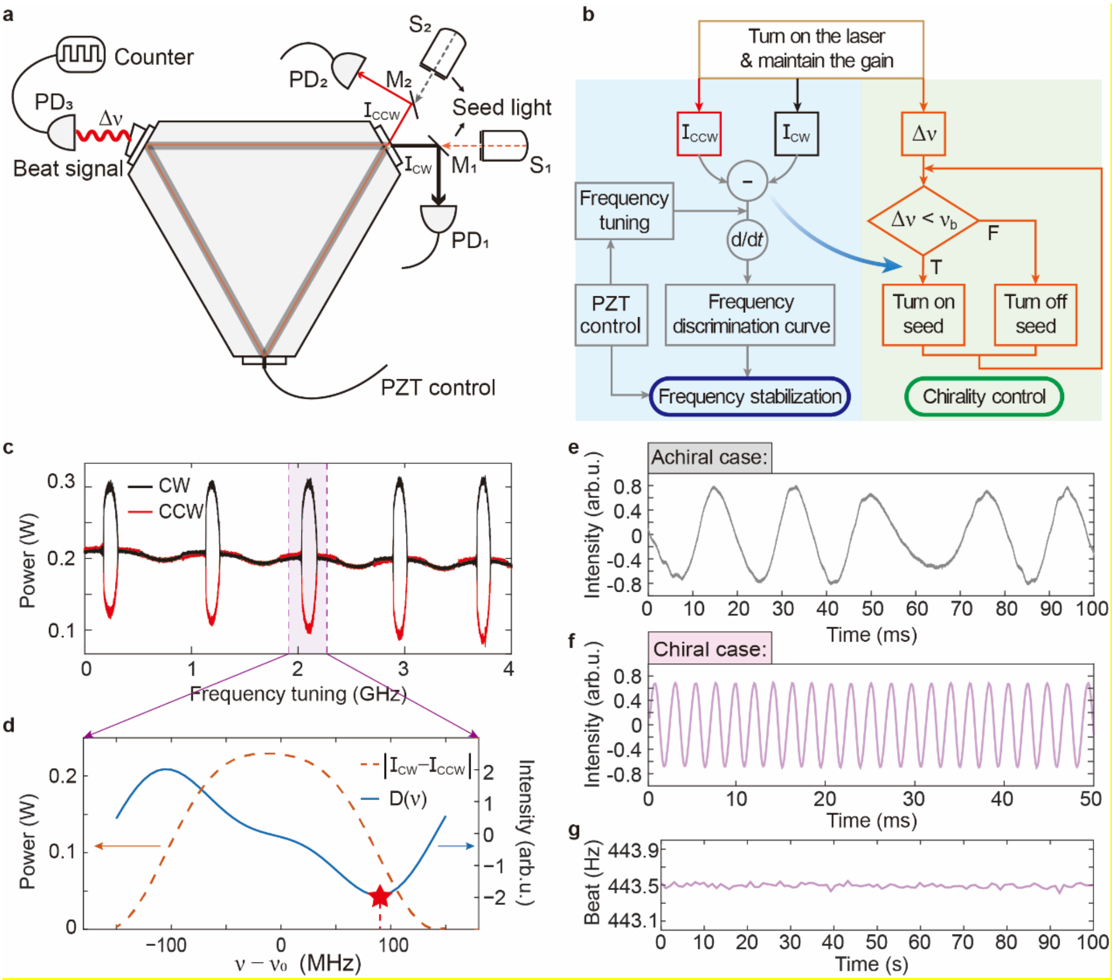

Fig. S5| Raw output signals and control strategies of the chiral RLG. a, Schematic of the signal readout and chirality control for the chiral RLG. PD1, PD2, and PD3 are photodetectors, measuring the CW laser intensity (I_{CW}), CCW laser intensity (I_{CCW}), and the beat signal $\Delta\nu$, respectively. The beat signal is then shaped and fed into a frequency counter. M_1 and M_2 are beam splitters. S_1 and S_2 are seed sources. PZT: piezoelectric transducer. **b**, Flowchart of the frequency stabilization and chiral control protocol. **c**, Full-range frequency tuning curves of laser intensity. Black and red curves represent the output power in the CW and CCW directions, respectively. The periodic pattern of chiral SSB indicates traversal of multiple longitudinal mode spacings during the unidirectional sweep of the PZT. **d**, Evolution of the intensity difference (orange curve) and the corresponding discrimination signal $D(\nu)$ (blue curve) as a function of laser frequency. The red star denotes the minimum of $D(\nu)$. **e**, Beat signal at a rotation rate of 0.04 °/s when the RLG is in the achiral state. **f**, Beat signal at the same rotation rate (0.04 °/s) when the RLG is in the chiral state. **g**, Continuous beat frequency over 100 seconds when the RLG is operated at the chiral state and stabilized at the point marked by the red star in panel **d**.

S4: Control strategies of the chiral RLG based on its output signal

Maintaining the stability of the operating point and the chiral state is crucial for acquiring high-quality experimental data from the laser gyroscope. Figures **S5a** and **S5b** illustrate the experimental setup and the control methodology, respectively. The frequency stabilization scheme and the chiral control protocol are detailed below:

Frequency Stabilization Method: Upon the laser is turned on, the PZT is firstly swept unidirectionally. The DC photodetectors PD1 and PD2 simultaneously record the intensities of CW and CCW laser modes, yielding the full-range mode sweeping curves (Fig. S5**c**). Concurrently, the absolute value of the intensity difference, $\Delta I = |I_{\mathrm{CW}} - I_{\mathrm{CCW}}|$, is computed in real-time via logic circuits. After noise reduction of the raw data, the corresponding PZT control voltages (V_{i}) at the extremum points of ΔI are recorded. The median of these voltages, V_0, is identified.

Subsequent fine frequency stabilization is performed around V_0. The orange curve in Fig. S5**d** shows the intensity difference ΔI around V_0; its derivative, the discrimination signal $D(v)$ (blue curve), is used for frequency stabilization. $D(v)$ is processed (smoothed and amplified) to precisely locate its minimum (red star, Fig. S5**d**). During operation, the frequency of the RLG (i.e., the operating point) is locked to this minimum by finely adjusting the PZT (displacement ~1 nm).

The sum of I_{CW} and I_{CCW} is also monitored in real-time to maintain gain stability by keeping the total intensity constant.

Once again, we extend our sincere gratitude to all the reviewers for their constructive feedback. Your invaluable comments and suggestions have significantly strengthened our manuscript. We believe that this improved version is suitable for publication in *Nature*.

List of main changes

Main changes in the main text

1) Page 2, Lines 54-59: we specified the full tuning range of the entire resonant cavity in the caption of Figure 1.
2) Page 2, Lines 71-75: We adjusted the text to clearly highlight the specific context of "chirality" used in our work concerning intensity symmetry breaking.
3) Page 4, Lines 84-91, Page 9, Lines 176-184 and Page 15, Lines 292-299: we rederived the theoretical model and added more explanations.
4) Page 5, Lines 96-99: we included the clarification of the parameter of nonlinear coupling coefficient.
5) Page 5, Fig. 2: we replotted Fig. 2 with explicit experimental parameters indicated on the required horizontal axes.
6) Page 5, Lines 104-111: we added essential notes to the caption of Fig. 2 as suggested.
7) Page 7, Lines 140-143: we thoroughly revised the manuscript to reflect the correct device parameters (125 mm side length, 800 MHz FSR).
8) Page 7, Fig. 3: we adjusted the color scheme in Fig. 3 and added a clarification in the caption.
9) Page 7, Lines 155-174: we revised the relevant description about the phrase "control paradigm" and provide detailed control steps.
10) Page 10, Fig. 4: we added the achiral RLG response to Fig. 4 and removed the former "Ideal Sagnac response" line from Fig. 4b to avoid redundancy and potential confusion.
11) Page 11, Lines 211-219: we improved the discussion of Fig. 4b, now it is more comprehensive.
12) Page 13, Lines 265-273: we included a discussion on the potential applications as on-chip solid-state sysmems.
13) Page 14, Lines 276-284: we further evaluated the effects of temperature variations in the Methods.
14) Related references have been added as Refs.[3-8, 13, 14, 48-52].

Main changes in the Supplementary Materials

15) Supplementary Materials, Section S1: we updated and provided additional explanation on the theoretical analysis and the complete derivation. A complete parameter Table S1 was also added.
16) Supplementary Materials, Section S2: we improved the description of the calculation of nonlinear coefficient and provided more specific references.
17) Supplementary Materials, Section S4 and Fig. S5: we added a comprehensive step-by-step protocol to include specifics on operating point selection, frequency tuning, and seed light injection. The added supplementary figure shows that we employed a specific strategy to systematically induce the desired chirality.
18) Supplementary Materials, Section S5 and Fig. S6: we added an analysis of bias stability in the chiral RLG.

Responses to the comments of Referee #1

I thank all the authors for their careful and thorough responses to the reviewers' comments. Excellent work! I believe the concerns have been successfully addressed, and the manuscript is a perfect fit for Nature.

Response: We thank the reviewer for the positive and encouraging comments. We are pleased that our responses have satisfactorily addressed the reviewers' concerns, and we appreciate your time and consideration of our manuscript.

Responses to the comments of Referee #2 and #3

General comments

The manuscript has undergone significant revisions following the first round of reviewers. However, some of the major issues we previously raised remain unresolved. We also compared our comments with the ones raised by the other referee, finding more than one point of contact. Carefully reading all the submission material and cross-checking among the different versions, including the Supplemental Material, the newly added sections in the methods, and, in particular, the coherence among simulations, theoretical model and relative plots, and experimental findings, we identified some inconsistencies in detail that prevent the manuscript from being accepted for publication in Nature.

The developed model of the RLG is not completely consistent with the reported experimental parameters. The latter are treated in a very qualitative manner, preventing the reader from understanding how the simulations, the analytical model, and the experimental features can be viewed under a unified framework. For details on our perspective, please read items 1.b, 2, 3, and 4 below.

The inconsistency found by the other referee regarding the geometrical factor and the reported construction parameters in the first version raises a serious concern about the accuracy in preparing the entire manuscript. In the first report, we didn't go into too many details on some of the "main comments" we raised. We regret to say that the authors missed to solve some of them leaving the level of discussion too qualitative. We have tried to evidence in the following the most critical points.

Response: We thank the reviewers for all these technical details. Their suggestions have enhanced the completeness and further improved the presentation clarity of our manuscript. In accordance with their suggestions, we have carefully checked again the simulations throughout the paper, confirming their overall consistency and alignment with our experimental findings. Specifically, based on Lamb's self-consistent equations for ring lasers, we have made meticulous adjustments to our theoretical simulation parameters and confirmed that our improved simulations provide a quantitative description and reasonable interpretation of essential new findings in our experiment. Also, we have now explicitly specified the side length (125 mm) and the total cavity length (375 mm) of the gyroscope in our work.

We note that two reviewers have already expressed full satisfaction with our previous round of revisions, particularly regarding the experimental results. In this revision, our primary focus thus is to further improve the theoretical model to find a more satisfying agreement with our experimental new findings. A detailed, point-by-point response to each of the issues raised will be given below.

As also appreciated by the other two reviewers, we would like to stress that the main findings of our work are the first realizations of a chiral laser gyroscope and its striking properties of breaking the lock-in limit suffered by traditional devices. We expect that our findings can lead to not only new devices for next-generation gyroscopes, but also exciting opportunities for more theory works on chiral ring-laser systems. (e.g., More efforts on exploring its microscopic mechanisms, more studies of the impacts of more practical issues, and more generalizations of our present device structure or design, which however are well beyond the scope of this present work.)

Comments to replies to main comments

Comment #1. We asked to include "in the manuscript a detailed description of the relation among cavity detuning, RLG working point (e.g. pump power and gas pressure) and the non-linear parameter ξ. The interplay between these experimental quantities is evident all over the paper, but an explicit, auto-consistent analysis is missed."; Referring to

a. the connection (Fig.1f) between non-linear coupling and frequency separation and the ratio between the intensities of CW and CCW beams;

b. the relation between α (net gain coefficient) and pump current (Fig.2c-d); the relation between ξ and tuning frequency (Fig. 2d-e).

a. We understand that Fig. 1**f** represents a behaviour and not an analytical plot, but citing Eq.(4) does not give an idea of the assessed linear dependence between the frequency splitting and the intensity difference. In addition, the equation for η, given in the reply to our comment, should have been inserted in the manuscript.

b. Fig.2 shows several issues. First, to correctly compare the simulations with the experimental data, the plots need to have the same parameters on both axes and the same scales. How can the reader compare the scale of α, given in Hz, with the pump current, given in mA? How can we compare different vertical scaling? How can the reader convert ξ, that is adimensional, into Hz? If in c and e the intensity is a measured one, it cannot be in arb.u.! The caption reports that plot b has been obtained by setting ξ=1.09, while plot d refers to α=1200Hz. If so, the graphs are not consistent! The intensity difference at α=1200Hz in b is roughly 3(black line just below 4, red one below 1), while at ξ=1.09 in d the difference looks more than 5 (black line close to 6, red one well below 1). The text reports that α and the pump current are proportional. From the caption, one reads that 1200 Hz corresponds to 0.6 mA, but at 0.6 mA in c, the red curve is higher than the red curve in b at 1200 Hz. Moreover, the bifurcation in b happens around 700 Hz; if the two quantities are truly proportional in the plotted range, the bifurcation should appear, in c, around 0.37 mA and not close to 0.5 mA, where it is now. By the way, the symbol ν, pedex free, appears in the caption of Fig.2 for the first time, and then in the caption of Fig.4, while it is defined in the text at line 221, if they are the same quantity.

Response #1

Reply to 1a: We thank the reviewer for this suggestion. First, we have adjusted the details of Fig. 1f and explicitly stated in its caption that under the chiral state, the frequency splitting is proportional to the intensity difference. A related explanation has also been added in the main text at line 189. Furthermore, since the variable η involves numerous parameters, and following the editor's advice to avoid excessive length in the main text, we have provided the complete equation for η and detailed related descriptions in the Supplementary Material:

According to the equations (S4) and (S5), the nonlinear frequency pulling coefficient η can be written as:

$$\eta = \rho - \tau = -g\frac{c\kappa}{2L}\left[\frac{dZ_{\mathrm{i}}(\varepsilon)}{d\varepsilon} + \frac{\varepsilon}{\kappa^2+\varepsilon^2}Z_{\mathrm{i}}(\varepsilon)\right] \tag{S6}$$

where g is the gain factor, c is the speed of light, L is the length of the laser cavity, κ is the ratio of the homogeneous broadening to Doppler broadening, $Z_{\mathrm{i}}(\varepsilon)$ is defined as the imaginary parts of the plasma dispersion function $Z(\varepsilon)$, and ε is the frequency parameter.

Reply to 1b: We appreciate the reviewer's valuable comments. To achieve more precise alignment with the experimental data, rather than just a qualitative trend analysis, we have carefully recalibrated and unified the theoretical model and simulation parameters. We have eliminated the ambiguous "arb. u." notation and adopted actual power units (μW). The inconsistencies in Fig. 2 and all other simulation plots have now been resolved, and the results show good agreement.

i) Regarding the linear relationship and unit consistency between α and the pump current: Besides revising the description of the linear relationship in the main text, we have added a quantitative analysis of their relationship in the Supplementary Material. Based on this, we unified the relevant horizontal axes in Fig. 2, and the results show good agreement.

Detailed explanation added to Methods:

Relationship between the gain coefficient α and pump current I_{p}

The laser gyroscope operates under a constant-voltage (~520 V) DC pump source. Therefore, the gain is increased by raising the pump current. Specifically, the threshold pump current of the system is I_{p} = 0.29 mA. This gain corresponds to the net cavity loss rate $\alpha_{\mathrm{th}} = \gamma_{\mathrm{th}} = -\log(1-\delta)/T_{\mathrm{rt}} = 5.435\times10^4$ Hz, where δ = 68 ppm is the total cavity loss and $T_{\mathrm{rt}} = \Delta L/c$ is the roundtrip time of the laser inside the cavity (ΔL is the cavity length, c is the speed of light). Under small-signal conditions, the gain is approximately linear, and the gain–current relationship can be estimated by the scaling factor $\chi = \alpha/I_{\mathrm{p}} = \alpha_{\mathrm{th}}/I_{\mathrm{pth}} = 1.875\times10^5$ Hz/mA.

ii) Regarding the nonlinear coupling coefficient ξ: We have emphasized in the text that ξ is dimensionless, but we acknowledge that it is not strictly linearly related to the cavity frequency (the horizontal axis in Fig. 2e). Overall, since ξ can be continuously tuned via the cavity frequency, the phase transition behavior from achiral to chiral states can be basically correlated between Figs. 2d and 2e. We have emphasized this point in the revised main text (Lines 123~126).

"To facilitate a direct comparison with experimental data, we also illustrate in Figs. 2**b** and 2**d** the symmetry-breaking process by varying the pump current I_{p} and nonlinear coupling strength ξ independently, along the dashed lines in Fig. 2**a**. The corresponding experimental data is shown in Figs. 2**c** and 2**e**, where ξ is finely controlled by the cavity tuning."

Through parameter correction and step-by-step revision, we recognize that a more rigorous and precise theoretical analysis indeed makes our work more convincing. Furthermore, to ensure transparency in the research process, **we have uploaded the codes for all simulation models used in this work during this revision.**

iii) The inconsistency in the figures mentioned has been resolved by recalibrating the simulation parameters. Regarding the symbol 'ν', its first appearance has now been placed at line 88 in the main text for clarity:

"…where $\tilde{E}_{1,2}(t) = E_{1,2}(t)\exp[-i(\nu t+\mu_{1,2}(t))]$ represent the complex electric fields of the CW and CCW waves, with time-dependent amplitudes $E_{1,2}(t)$ and phases $\mu_{1,2}(t)$; ν is the resonant frequency of the ring cavity (i.e., the operating point of the RLG)…"

Comment #2. There is still some missing information to understand the physics of the system. In particular, from the graph in Fig. S5c, it can be inferred that the system is intrinsically asymmetric. A higher intensity of the CW beams looks like a preferred state. Where does this feature come from? The scheme shows two additional laser sources coupled to both propagation directions. It is unclear why feedback is provided and/or required on both beams.

Response #2: We thank the reviewer for pointing out this aspect of Fig. S5c of the Supplementary Material. The reason why the higher intensity of the clockwise (CW) beam appears as a preferred state is that, in this specific case, the gyroscope was rotating clockwise at a constant rate of 0.04°/s. Consequently, the chiral state corresponding to the rotation direction becomes dominant. To minimize reader confusion and present a clearer physical picture, we have further clarified the rotational state of the gyroscope in the figure captions in the revised version.

On the other hand, the seed lights are used to control the chirality of the gyroscope. Since the chirality of this gyroscope is generated via spontaneous symmetry breaking, it is possible that it enters the chiral state with stronger counter-clockwise (CCW) intensity even under clockwise rotation, and vice versa. To handle both scenarios reliably, the safest approach is to introduce a seed light for feedback in both propagation directions, allowing us to steer the gyroscope towards the desired chiral state.

Revision on the captions of Fig. S5:

“**c**, Full-range frequency tuning curves of laser intensity under clockwise rotation at 0.04 °/s. Black and red curves represent the output power in the CW and CCW directions, respectively. The periodic pattern of chiral SSB indicates traversal of multiple longitudinal mode spacings during the unidirectional sweep of the PZT. Attributed to the clockwise rotation direction, the RLG consistently favors the chiral state with stronger CW mode intensity during cavity length tuning.”

Comment #3. We asked to include in the manuscript a discussion on the effect of the intensity unbalance on fringe contrast and the SNR of the instrument (see Comment 3). The authors address the point in their reply, but it is not included in the actual manuscript. By the way, in their reply the authors use unprecise values for the output powers of the beams: as can be seen in Fig. 4a, at the operating point v3(“the point of maximum frequency bias") the output powers of the CW and CCW beams are slightly less than 6μW and slightly higher than 2μW respectively, and not approximately 5μW and 3μW as reported by the authors. Moreover, while for 5μW and 3μW is correct that the beat note amplitude would reduce by 3.2%, the reported formula is wrong the correct one being $\sqrt{I_1 I_2}$. The beat note amplitude for the correct powers at “the point of maximum frequency bias”, then, reduces by more than 10%.

Response #3: We thank the reviewer for their thoroughness. To enhance the robustness of the manuscript, we have added a discussion regarding the effect of chirality on the signal-to-noise ratio (SNR) of the gyroscope's beat note in the main text. At our chosen operating point of maximum frequency bias, the chiral state leads to output powers of approximately 5.62 μW and 2.34 μW for the CW and CCW beams, respectively. This results in a reduction of the beat note amplitude by approximately 10%. Crucially, this reduction remains well above the detector's noise floor. Therefore, as indicated in our previous response, the intensity asymmetry does not adversely affect the readout of the gyroscope's beat signal. We have incorporated the following discussion into the main text:

"Moreover, although the intensity asymmetry at this operating point reduces the interference fringe contrast by approximately 10%, leading to a decrease in the signal-to-noise ratio from 35.5 dB under achiral conditions to 34.9 dB under chiral conditions, this value remains well above the typical SNR limit (~20 dB) required for high-precision laser gyroscope frequency counting. Therefore, such a chiral bias does not adversely affect the readout of the gyroscope signal."

Comment #4. The authors amended the laser equations in the Supplementary Material and in the Methods section only. These amended equations are not used in the actual version of the main text. In particular, the new set of coupled equations(S1)-(S3) predicts Eq.(S8) for the instantaneous frequency, but Eq.(S8) is never used in the main text. On the contrary, the theoretical model in the main text is still based on Eq.(3). The link between Eq.(3) and Eq.(S8) is not clear, since they exhibit exact agreement in the achiral case only (i.e., same intensities) and not in the much more interesting achiral case that is the focus of the regime actually investigated. Moreover, it is not clear what the authors mean by "steady-state chiral solutions to the amplitude equations(S2)" just before Eq.(S4). Do the authors mean that the equations(S2) admit exact or approximate steady-state solutions for the intensities?

Response #4: We thank the reviewer for their meticulous comments regarding the theoretical model. In the latest version of the manuscript, we have fully adopted the theory based on Lamb's self-consistency equations and removed the previous matrix approximation method. The expression for the gyroscope's beat frequency, derived from the self-consistency equations, is now presented in the main text Equation (2), and a detailed derivation is provided in the Methods section.

Concerning the phrase "**steady-state chiral solutions to the amplitude equations (S2)**" in the previous Supplementary Material, it referred to the fact that the self-consistency equations **yield two sets of steady-state solutions: one achiral solution with $E_1 = E_2$, and another chiral solution with $E_1 \neq E_2$**. To avoid any potential ambiguity, we have removed this phrasing.

Comments to reply to textual comments:

Comment #h. We asked the authors to clarify the units used for the plots in Fig. 2. In their reply to our comment, the authors write: "Based on the comparison with our experimental data(Fig. 4b), we determined that the backscattering coupling coefficient r is approximately 30 Hz. Consequently, all linear frequency parameters in our model required scaling. Specifically, the linear gain coefficient a has also been scaled to maintain consistency with the physical system." It is not clear what the authors mean, given that the new horizontal axis for the plot in Fig. 2b has been rescaled by a factor of 1500 Hz compared to the previous version. Moreover, in the same response, the authors say:"The theoretical plots in Fig. 2 are now based on Eq.(4) in the Methods section, which is derived from Eq.(1) using the separation of variables method for the amplitude equations." However, apart from the already discussed rescaling of the horizontal axis, there are no visible differences between the theoretical plots in Fig. 2 in the present version of the manuscript and the previous one. This comment is very much related to the main comment 1-b given above.

Response #h: We thank the reviewers for this valuable comments. Regarding the units in Fig. 2, the inconsistency has been resolved by recalibrating the simulation parameters. The backscattering coefficient r of approximately 30 Hz was converted from the experimentally measured lock-in threshold under achiral conditions. The parameter α has been re-determined based on the gain-current relationship (see our response to Main Comment 1.b). We have now completed meticulous recalculations and revisions for Fig. 2.

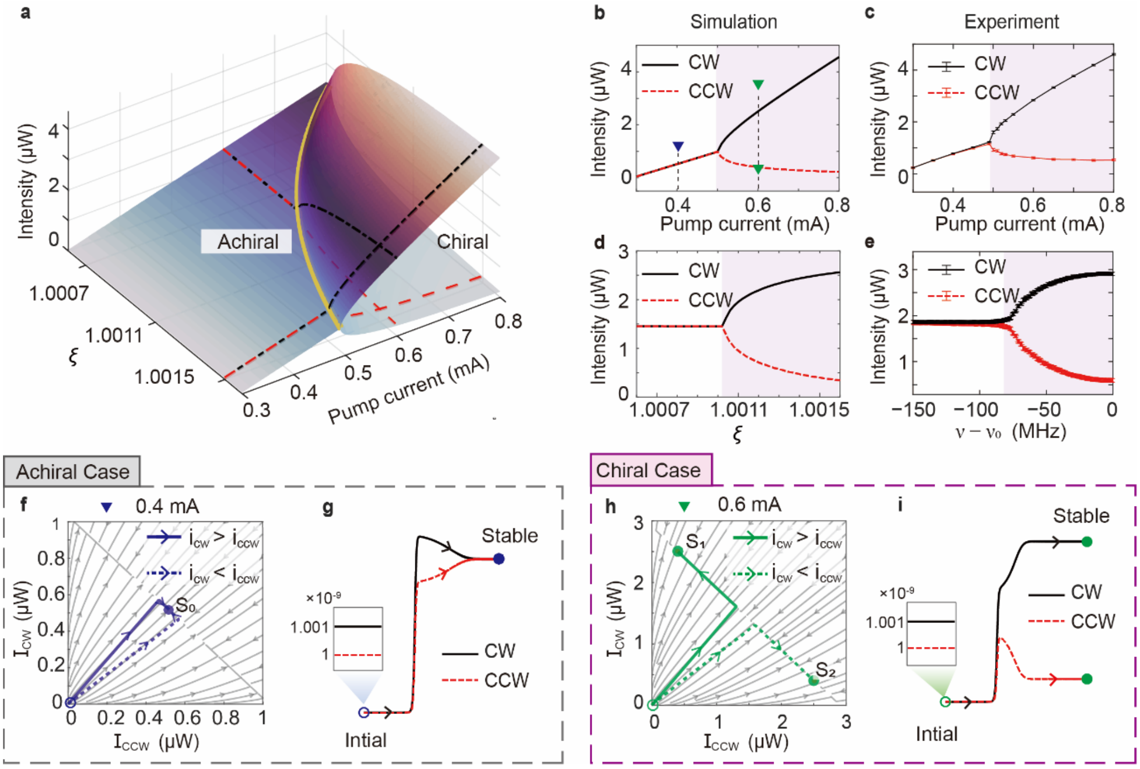

Fig. 2| Theoretical analysis of SSB in the ring laser. a, Phase diagram in two-parameter space (ξ: nonlinear coupling coefficient, α: net gain coefficient) demarcating symmetric (left of the yellow curve) and chiral SSB states (right). **b,** Simulated and **c,** experimental results of pitchfork bifurcation in CW/CCW intensities by increasing gain at $\xi = 1.0015$ and $\nu = \nu_0$, respectively; ν_0 is the gain center of Ne[20]. **d,** Simulated and **e,** experimental results of pitchfork bifurcation by increasing the nonlinear coupling coefficient (or tuning frequency) at the pump current $I_p = 0.6$ mA, respectively. The shaded regions in **e** represent the fluctuation range of the laser light intensity (i.e., the standard deviation of the measurement results). **(f, h),** Simulations of **f,** the symmetric state ($I_p = 0.4$ mA) and **h,** the chiral SSB state ($I_p = 0.6$ mA): **f,** Phase diagram of the intensity evolution with one stable point (S_0); **h,** Phase diagram of the intensity evolution with two stable points (S_1 and S_2), where i_{cw} and i_{ccw} are the minute initial intensities of the CW and CCW modes, respectively. **(g, i),** Schematic illustrations of the evolution of the CW and CCW mode intensities from the initial to the stable state under **g,** symmetric and **i,** chiral SSB conditions. In both **g** and **i**, i_{cw} exceeds i_{ccw} by 0.1%.

Comment #j. In response to our Comment#j the authors say that in Fig. 2g and 2i the horizontal axes "does not represent the physical running time of the RLG but rather the convergence time of the numerical solution. To avoid misunderstanding, we have modified the labels on the horizontal axes in Figs.2g and 2i, accordingly." The authors should explicitly state in the caption of Fig. 2 that the plots f-i are simulations. Moreover, the units and ticks on the horizontal axes should be reintroduced. The use of arb.u. for intensities is not convincing, especially because the numbers mimic actual values in μW as it appears from the authors' reply to main comment 3.

Response #j: We thank the reviewer for these suggestions. We have recalculated the numerical simulation results for Figs. 2f and 2h, now correlating the simulated intensities with the actual experimental results in ‘μW’. Furthermore, to avoid ambiguity, Figs. 2g and 2i, which demonstrate how minute initial value differences lead to distinct steady states under achiral and chiral conditions, **have been replaced with schematic diagrams**. Corresponding clarifications have been added to the figure caption:

“**(f, h),** Simulations of **f,** the symmetric state ($I_p = 0.4$ mA) and **h,** the chiral SSB state ($I_p = 0.6$ mA): **f,** Phase diagram of the intensity evolution with one stable point (S_0); **h,** Phase diagram of the intensity evolution with two stable points (S_1 and S_2), where i_{cw} and i_{ccw} are the minute initial intensity of the CW and CCW modes, respectively. **(g, i),** Schematic illustrations of the evolution of the CW and CCW mode intensities from the initial to the stable state under **g,** symmetric and **i,** chiral SSB conditions. In both **g** and **i**, i_{cw} exceeds i_{ccw} by 0.1%.”

Comment #o. The equation for the beat frequency in the authors' reply to our comment#o should be included in the manuscript. Moreover, the choice of integration time T should be clarified.

Response #o: We thank the reviewer for this valuable suggestion. We have comprehensively revised the theoretical section in the main text. The beat frequency equation derived from the self-consistency equations is now presented as Equation (2) in the main text. In the Methods section, we detail the derivation process for the beat frequency and explicitly define the integration time $T = 2\pi/\omega_B$:

In the main text (Lines 176~178):

Compared with traditional two-frequency RLGs, the beat frequency of the chiral RLG needs to be modified. The frequency difference between CW and CCW modes can be obtained by solving the imaginary parts of Equation (1) (the derivation can be found in the Methods):

$$\Delta v = \sqrt{[\eta(I_{\mathrm{cw}} - I_{\mathrm{ccw}}) + 2\Omega_S]^2 - \left(\frac{I_{\mathrm{cw}}}{I_{\mathrm{ccw}}} + \frac{I_{\mathrm{ccw}}}{I_{\mathrm{cw}}} + 2\right) r^2} \tag{2}$$

In the Methods (Lines 328~329):

The beat frequency Δv is derived by taking the time average (i.e., $T = 2\pi/\omega_B$) of the derivatives of the phase difference[41]:

$$\Delta v = \frac{1}{T}\int_0^T \frac{\partial \Delta u}{\partial t} dt = \frac{4\pi}{T} = 2\omega_B = \sqrt{A^2 - B^2}$$
$$= \sqrt{[\eta(I_{\mathrm{cw}} - I_{\mathrm{ccw}}) + 2\Omega_S]^2 - \left(\frac{I_{\mathrm{cw}}}{I_{\mathrm{ccw}}} + \frac{I_{\mathrm{ccw}}}{I_{\mathrm{cw}}} + 2\right) r^2}\,. \tag{11}$$

Comment #s. In Comment #s we asked to provide “an estimation for the back-scattering ratio r to justify the assumption of a small quantity. "Even if in their reply to our comment, the authors say that “In the revised derivation, it is no longer necessary to approximate or ignore the backscattering coefficient r", the manuscript would benefit from the inclusion of an estimate for the backscattering coefficient. Note that the value reported in the reply (30 Hz) is not included in the manuscript. Moreover, “smallness” of r can be assessed only when compared to the(rotation-dependent) Sagnac frequency Ω_S. To facilitate the comparison, we suggest including an estimate of the scale factor S and/or typical values of Ω_S) for relevant values of rotation.

Response #s: We thank the reviewer for this valuable suggestion. We have added relevant discussion in the main text, comparing the lock-in threshold of ~66 Hz caused by backscattering with the frequency bias of ~364 Hz induced by chirality. This demonstrates that under chiral biasing, the gyroscope operates far from the lock-in region and achieves a nearly linear response to external rotation rates. We have added the following discussion in the main text:

"Considering a typical value of the backscattering coefficient $r = 30$ Hz, for a chiral RLG operating at the point of maximum frequency bias (e.g., $\nu = \nu_3$ in Fig. 4**a**) with intensity ratio $I_{\mathrm{cw}}/I_{\mathrm{ccw}} \approx 2.4$, the introduced frequency bias is about 364 Hz, which is far greater than the lock-in threshold $\sqrt{\left(\frac{I_{\mathrm{cw}}}{I_{\mathrm{ccw}}} + \frac{I_{\mathrm{ccw}}}{I_{\mathrm{cw}}} + 2\right)}r \approx 66$ Hz. Therefore, the chiral RLG will always have a real and nearly linear frequency response with rotation, provided that $\eta(I_{\mathrm{cw}} - I_{\mathrm{ccw}})$ and Ω_{S} have the same sign."

Comment. Moreover, the data complementing the manuscript are still not of immediate use. In particular, the authors say in their reply: "The data file named "e-increasing coupling.CSV" for Fig. 2e records the optical intensity variation under continuous linear frequency tuning. This data was acquired directly from an oscilloscope; therefore, the first column represents the time(in seconds) recorded by the oscilloscope, which corresponds to the frequency shift during the continuous tuning process." Note that this discussion is not included in the text and should be added. By the way, without an indication of the constant rate of the frequency tuning, it is not possible to relate the "scanning time" to the values of the frequency on the horizontal axis of Fig. 2e. Moreover, in all the files, units for the intensities are missing or are different from the ones reported in the actual plot. For example, in the data for Fig. 2 the units for the intensities are missing and the values are not in the range showed on the vertical axis of the plots in Fig. 2c and 2e.

Response: We thank the reviewer for this comment regarding data accessibility. The reviewer correctly points out that the originally uploaded raw oscilloscope traces are not directly comparable to the figures in the manuscript. This is because they require several standard preprocessing steps to convert the raw voltage-time data into the analyzed data presented in the figures. To address this and ensure immediate usability, we have now uploaded a new dataset in the folder named "Processed_Data_for_Figures" alongside the original raw data. The processing involved:

1. Converting recorded voltages into the optical power (i.e., μW) shown in the figures.
2. Converting scanning time into the frequency tuning (i.e., MHz) shown in the figures.
3. Removing instrument offset to establish a true zero baseline.

To ensure full transparency and reproducibility, we have provided a detailed protocol as a README.txt file within the new dataset to generate the figure-ready data from the raw files.

New comments in view of the amended text

Comment #1. At line 179, the frequency Ω_S is introduced. The link with ν_S introduced at line 37 is not clear.

Response #1: We thank the reviewer for this careful check. The two symbols indeed represent the same physical quantity: the frequency shift induced by the Sagnac effect. We have unified the notation throughout the manuscript and now consistently use Ω_S.

Comment #2. At lines 96-97 of the manuscript, the authors say that:"a is proportional to the pump current within the gain range (0.4~0.8 mA) studied in this work". However, as can be clearly seen from Fig. 2c just below the experimental data range is larger (at least 0.2-0.8 mA). Moreover, where is it possible to see the proportionality between a and the pump current? See the comment to Fig. 2 above for the proportionality issue.

Response #2: Thanks for the valuable comments. After carefully re-analyzing the experimental data, we have now determined the threshold pump current to be 0.29 mA. Consequently, the gain–current data presented in Figure 2 consistently falls within the range of 0.3–0.8 mA. Under small-signal conditions, the gain exhibits a linear dependence on the current. In the revised manuscript, we have not only emphasized this point in the main text but also included a relevant quantitative estimation in the Methods section.

Revision on the Main text:

"In particular, α is proportional to the pump current I_p (i.e., $\alpha = \chi I_\mathrm{p}$ and $\chi = 1.875 \times 10^5$ Hz/mA, see Methods) within the gain range (e.g., 0.3~0.8 mA) studied in this work ...".

Revision on the Methods:

Relationship between the gain coefficient α and pump current I_p

"The laser gyroscope operates under a constant-voltage (~520 V) DC pump source. Therefore, the gain is increased by raising the pump current. Specifically, the threshold pump current of the system is $I_\mathrm{p} = 0.29$ mA. This gain corresponds to the net cavity loss rate $\alpha_\mathrm{th} = \gamma_\mathrm{th} = -\log(1-\delta)/T_\mathrm{rt} = 5.435 \times 10^4$ Hz, where $\delta = 68$ ppm is the total cavity loss and $T_\mathrm{rt} = \Delta L/c$ is the roundtrip time of the laser inside the cavity (ΔL is the cavity length, c is the speed of light). Under small-signal conditions, the gain is approximately linear, and the gain–current relationship can be estimated by the scaling factor $\chi = \alpha/I_\mathrm{p} = \alpha_\mathrm{th}/I_\mathrm{pth} = 1.875 \times 10^5$ Hz/mA."

Comment #3. At line 141, we suggest specifying whether 125 mm is the cavity side length or the total length.

Response #3: We thank the reviewer for this comment. The side length of the triangular gyroscope cavity is 125 mm. We have clarified this point in the manuscript:

"…we fabricated a triangular He-Ne^{20} RLG with a side length of 125 mm."

Comment #4. At line 176, it is not clear what the authors mean by "approximate gain clamping condition" used to derive Eq.(2). Moreover, for self-consistency, the authors should add how this approximation is implemented in relation to the equations in the Supplementary Material (Eqs.(S1)-(S8)).

Response #4: The gain clamping condition is a linear approximation for the dual-mode model of the RLGs, which drew from Vahala's work (Nature 576, 65–69 (2019)), which provided an comprehensive but approximate result. To enhance the overall theoretical consistency of the manuscript, we have removed this linear approximation theory. The analysis is now entirely based on the derivation from Equation (1) in the main text.

Comment #5. Eq.(3) is not consistent with Eq.(S8) (see also below comment 10).

Response #5: In the latest revised version, we have replaced the original Equation (3) with Equation (S8).

Comment #6. Throughout the text, the symbol v is used, but its definition is not clear. In the main text, the frequency v is mentioned for the first time at line 221 as "the operating frequency of the RLG". It is not entirely clear what this actually indicates, and whether there is a connection to the resonance frequency of the ring cavity, ω, which is defined at line 87.

Response #6: The symbol v represents the operating point of the gyroscope, which corresponds to the resonant frequency of the ring cavity. We have unified the notation as the symbol v throughout the text.

Comment #7. At line 278, the authors provide information on the stability for a cavity of length 0.375m, but the actual cavity length is 125 mm(line 141). Thus, the information provided by the authors may be misleading regarding the actual RLG geometry.

Response #7: We thank the reviewer for their thoroughness. The side length of the equilateral triangular ring resonator is 125 mm, corresponding to a perimeter of 0.375 m. We have clarified this relationship in the manuscript as mentioned in the response to the New comment **3** above:

"…For a total cavity length of 0.375 m, a temperature fluctuation of 0.1°C results in a length change of ΔL = 0.375 m × 2×10^{-8} /°C × 0.1°C = 0.75 nm."

Comment #8. After line 299, it is not clear why they need to introduce the functions f and g. As far as it is possible to follow the reasoning underneath, the two coincide with the expressions given in Eq.(4) unless there are unexpressed approximations apart from cosΔu=1. If so, please specify the approximate expression used for f and g.

Response #8: The functions f and g were initially introduced in the original text merely for notational convenience. We acknowledge that adding these functions could potentially cause confusion for readers. Therefore, in the revised derivation, we have removed these expressions to streamline the presentation:

Based on Equation (3), the Jacobian matrix of $\dot{E}_1$ and $\dot{E}_2$ is

$$J=\begin{bmatrix}\frac{\partial \dot{E}_1}{\partial E_1} & \frac{\partial \dot{E}_1}{\partial E_2}\\ \frac{\partial \dot{E}_2}{\partial E_1} & \frac{\partial \dot{E}_2}{\partial E_2}\end{bmatrix}=\begin{bmatrix}-3\beta E_1^2-\beta\xi E_2^2+\alpha & -2\beta\xi E_1E_2+r\\ -2\beta\xi E_1E_2+r & -3\beta E_2^2-\beta\xi E_1^2+\alpha\end{bmatrix}. \quad (5)$$

Comment #9. In Eq.(S8) the definition of the mean<> should be provided (see Comment#o). The link between Eqs.(S8) and(3) is not clear since they are consistent in the achiral case only. The discrepancy between the two methods in the chiral case should be quantified with reference to the actual data range studied in the manuscript.

Response #9: In the latest version of the manuscript, we have replaced the mean value <> with a definite integral specifying the upper and lower limits. The original Equation (3) was a comprehensive approximate result referencing the work of Vahala et al. Nature 576, 65–69 (2019), but it was not sufficiently accurate. Consequently, we now exclusively use the beat frequency result derived from the self-consistent equations and have removed the original Equation (3) and the associated matrix theory.

Comment #10. Fig. S4a is not consistent with Fig. 2d (compare the values of the intensities in the two plots for α=1200Hz) and ξ=1.07). By the way, the authors should explicitly state in the caption of Fig. S4 that the plots are simulations.

Response #10: We thank the reviewer for this valuable comment. Figure S4 has been replotted using the latest simulation model and parameters, ensuring consistency across all simulation results in the manuscript.

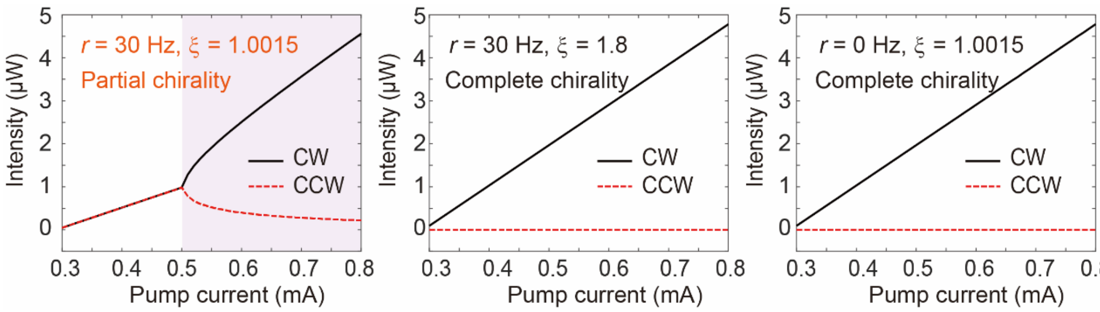

Fig. S4| Simulations of chirality features under different parametric configurations. α, ξ, and r denote the net gain coefficient, the nonlinear coupling coefficient, and the backscattering coefficient, respectively. The black solid lines / red dashed lines represent the intensity of CW/CCW laser modes.

Comment #11. In the Section. "Frequency stabilization method", when the authors say "its derivative, the discrimination signal D(v)", we suggest to specify that it is the derivative with respect to time.

Response #11: We thank the reviewer for this suggestion. We have made the corresponding clarification in the relevant section.

"Subsequent fine frequency stabilization is performed around V_0. The orange curve in Fig. S5**d** shows the intensity difference ΔI around V_0; and the blue curve is its derivative with respect to time, the discrimination signal $D(v)$, which is used for frequency stabilization."

Responses to the comments of Referee #4

The author has answered all my questions. I am satisfied with these responses and have no further questions.

Response: We thank the reviewer for the positive feedback and are pleased that our responses have addressed all the questions satisfactorily.

Responses to the comments of Referee #2 and #3

Referee #2 (Remarks to the Author):

Manuscript ID: AE12826
Title: Chiral laser gyroscopes breaking the lock-in limit
Authors: by Yuan-Hao Mao, Ji-Peng Xu, Hong-Teng Ji, et al.

General comment
The authors have solved most of the critical issues we have identified in our second report. However, we underline a possible small inconsistency that may require a further authors' check. the definition of Ω_S at line 37 may not be consistent with the use in Eq. (4) a factor 1/2 looks missing. Using the present formulas the frequency difference would be 2Ω_S.

We agree that the presented results are of wide interest for future application and studies on RLG and can be published, in the present form, in Nature.

Referee #3 (Remarks to the Author):

I co-reviewed this manuscript with one of the reviewers who provided the listed reports.

Responses:

We thank the Referee #2 for acknowledging that we have addressed the critical issues from the previous round and for the positive recommendation. We would also like to thank Referee #3 for co-reviewing the manuscript and for the time and effort dedicated to this process.

We appreciate the referee for pointing out this potential inconsistency about the definition of Ω_S. Upon re-examination, we agree that the definition need to be clarified to avoid any misunderstanding. The symbol Ω_S was intended to represent half of the beat frequency, i.e., the contribution of the Sagnac effect to a single laser mode (either clockwise or counterclockwise). Therefore, the original expression on line 37 indeed missed a factor of 1/2. We have revisited the relevant section to ensure consistency (line 39):

"This beating signal originates from the Sagnac effect[11,12], which causes a frequency splitting between a pair of clockwise (CW) and counterclockwise (CCW) laser modes (i.e., $\Omega_S = S\Omega/2$, where Ω_S is the mode frequency shift and S is a scale factor)."